Substructuring in flexible multibody dynamic models

Master thesis Mechanical Engineering

A.M. Palthe, s1375091

June, 2021

Summary

Theme park ride manufacturers use conventional ways to dimension their rides. Finite element (FE) analysis is used on each part separately and worst case quasi-static load cases are used to determine the maximum stress in the material. Amusement rides often have large motions, which introduce nonlinear equations of motion. Linear FE models cannot solve these equations, which leads to a high level of uncertainty. Therefore high safety factors are used, which means that parts are highly overdimensioned. The result is an overweight structure with unknown dynamic effects.

Multibody dynamic (MBD) analysis can account for large motions, but assumes all parts to be rigid. This thesis aims to determine a method to combine FE analysis into a MBD model, to obtain a flexible model which can be used for structures with large motions. The focus is on a specific class of theme park rides, named "rotating tower rides". These rides consist of a vertical tower rotating around its axis, with some type of moving gondolas attached. This is a common type of ride and is built by many different manufacturers. Predicting the loads and internal stresses accurately is a common difficulty, especially at the connection of the tower to the bearing. Amusement park Toverland has provided data of the Wirbelbaum, which is a ride of the type FlyingWheels by Metallbau Emmeln. This data shows that the tower-bearing connection is indeed a critical point in the structure and fatigue damage caused failure much sooner than expected.

This thesis compares results obtained with linear FE analysis with results obtained with flexible MBD analysis. For this purpose, multiple models are made of both the tower and the bearing in Matlab, Ansys and Adams. A static analysis is used to validate all models. However, since validation of the Adams model was unsuccessful, there is more emphasis on the method of applying flexible multibody analysis.

Two dynamic analyses are done. In the first, the rotation of the tower is constrained. Removing this large motion should lead to similar results from the FE model and the flexible MBD model. The second analysis includes this rotation and comparing these results shows the added value of using a flexible MBD analysis.

Finally, some recommendations are listed for further research.

Contents

1 Introduction

Before computers could be used to calculate the stresses and deformations in a structure, people relied on analytic solutions and the experience of engineers. If the structure was very complicated it needed a lot of simplifications, and therefore assumptions were made. This could lead to unexpected, expensive and even dangerous situations. Even the use of experiments leaves uncertainties and can lead to high costs, especially if a lot of iterations are needed.

The introduction of computers and especially finite element (FE) analysis in the 1950s enabled engineers to predict structural behaviour on a more detailed level [1]. Although at this time, FE analysis was so tedious that it was mainly used to verify a completed design or to study a failed structure. It took until the late 1970s for FE analysis to be used in the design stage [2].

Since then, available computational power has grown exceedingly, but the requirements of structures and thus of the simulations have increased as well. Detailed simulations can take a lot of time, which is especially inconvenient if multiple people or project groups are working simultaneously on the same structure.

Nowadays the use of FE models has become common practice. However, linear FE models assume small displacements and therefore cannot be used in case of large motions, as is common for amusement rides for example. For this purpose, multibody dynamic (MBD) analysis can be used. This type of analysis considers multiple bodies which are connected to each other by joints, influencing each others motions. However, implementing flexibility in a MBD analysis can be challenging.

This thesis aims to determine the added value of using flexible multibody dynamic models in the design of such a ride using a case study. A method to use FE models in a MBD environment is described, resulting in a flexible multibody dynamic model.

1.1 Finite element analysis

The foundation of finite element analysis, also called finite element method, is to divide a problem into a finite number of smaller problems, which is called discretisation. In spatial discretisation, a large structure is divided into smaller parts, called *elements*. Because these elements are very small, the displacement field can be approximated by low-order equations. The elements are connected to each other by *nodes* and the arrangement of elements is called a *mesh*. A FE analysis provides a nodal solution, which can be combined with the assumed field in the element to obtain the spatial variation of the solution. The finite element method can be used in many fields, but in this thesis only the application in structural mechanics is considered.

Different types of elements can be chosen, depending on the situation. Beam elements have two nodes, one at each end of the element. These elements use higher order interpolation functions, which enables them to account for bending and torsion.

Volumes can be modelled using solid elements. However, if the thickness of the structure is small compared to its other dimensions, shell elements are more suitable.

1.1.1 Substructuring in FE analysis

Substructuring is the division of the original structure into components to manage a large FE project [2]. This division should be located where parts have few interconnections to reduce the number of necessary equations. For each substructure a FE model is made and its equilibrium equation is considered (equation 1).

$$\mathbf{K}\mathbf{u} = \mathbf{P} \tag{1}$$

Equation 1 is rewritten to make the distinction between boundary displacements $\mathbf{u}_b$ and internal displacements $\mathbf{u}_i$, as shown in equation 2. Here, $\mathbf{P}_b$ is the vector of loads applied at the boundary nodes. Nodes where loads are applied are also considered boundary nodes.

$$\begin{bmatrix} \mathbf{K}_{bb} & \mathbf{K}_{bi} \\ \mathbf{K}_{ib} & \mathbf{K}_{ii} \end{bmatrix} \begin{bmatrix} \mathbf{u}_b \\ \mathbf{u}_i \end{bmatrix} = \begin{bmatrix} \mathbf{P}_b \\ \mathbf{0} \end{bmatrix} \tag{2}$$

This equation is rewritten to describe all displacements as a function of the stiffness matrix and the boundary displacements, as shown in equation 3.

$$\mathbf{u} = \begin{bmatrix} \mathbf{u}_b \\ \mathbf{u}_i \end{bmatrix} = \begin{bmatrix} \mathbf{1} \\ -\mathbf{K}_{ii}^{-1}\mathbf{K}_{ib} \end{bmatrix} \mathbf{u}_b = \begin{bmatrix} \mathbf{1} \\ \mathbf{\Psi} \end{bmatrix} = \mathbf{\Phi}_G \mathbf{u}_b \tag{3}$$

The columns of the Guyan reduction matrix $\mathbf{\Phi}_G$ contain the static displacement of the structure when one of the boundary nodes has a unit displacement, while the other dofs are fixed. These constraint modes for a

two node 2D beam are visualised in figure 1. The reduction matrix is used to obtain the reduced equilibrium equation, as shown in equation 4.

$$\boldsymbol{\Phi}_G^T \mathbf{K} \boldsymbol{\Phi}_G \mathbf{u}_b = \boldsymbol{\Phi}_G^T \mathbf{P}$$
$$\mathbf{K}_{red} \mathbf{u}_b = \mathbf{P}_{red}$$
(4)

This reduction process is called Guyan reduction and gives the same reduced stiffness matrix as static condensation, where a substructure is regarded as an element with many internal dof [2]. Therefore, substructures are also referred to as superelements.

The reduced equations of all substructures can be assembled into a global equation. This equation can be solved for the boundary dofs, which can be used to solve the substructure equilibrium equations.
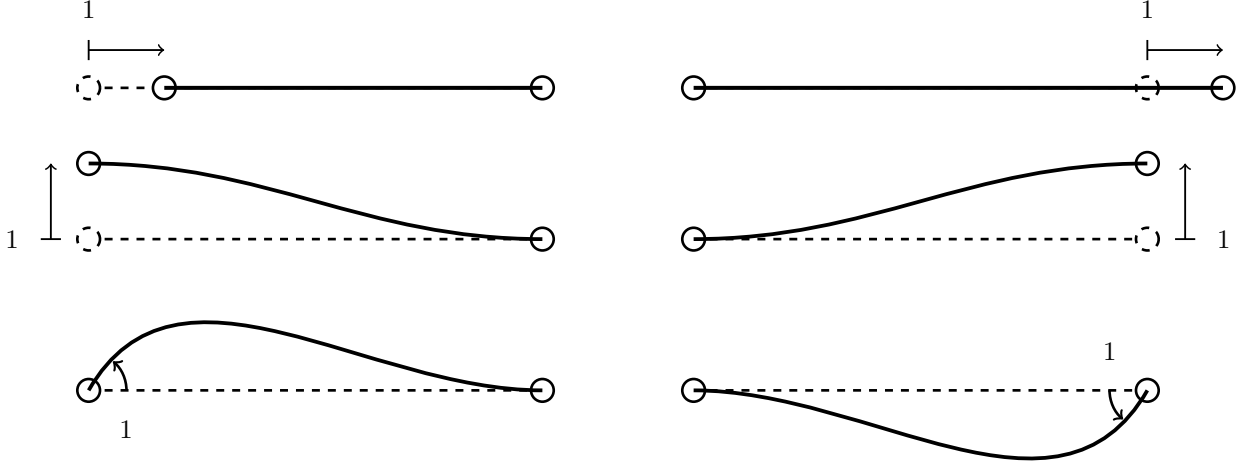

Figure 1: Static mode shapes of a 2D beam with both ends clamped

1.1.2 Dynamic substructuring

If the loading of a structure is time-dependent, its response is also time-dependent. Dynamic analysis is used to determine a structures natural frequencies and their mode shapes, but also to determine the response to transient loads. The equation of motion used in dynamic analysis is an elaboration of equation 1, as shown in equation 5. This equation includes the mass matrix $\mathbf{M}$ and the damping matrix $\mathbf{C}$ (which is often a fraction of the stiffness matrix). The time derivatives of the displacement are also included: the velocity $\dot{\mathbf{u}}$ and acceleration $\ddot{\mathbf{u}}$. The same reduction method can be used to obtain an equation which only depends on the boundary nodes.

$$\mathbf{M}\ddot{\mathbf{u}} + \mathbf{C}\dot{\mathbf{u}} + \mathbf{K}\mathbf{u} = \mathbf{P}$$
(5)

In dynamic substructuring, also known as component mode synthesis (CMS), modal synthesis and substructure synthesis [2], the model is divided into several parts which can be evaluated separately. Only the data at the interfaces is needed to evaluate the next part.

Many substructuring methods are available, of which the Craig-Bampton method is the most widely used method. It is very similar to the Guyan reduction, but includes internal vibration modes, or component modes, to account for both mass and stiffness. Equation 6 shows the Craig-Bampton transformation, where $\mathbf{q}$ is the vector of modal coordinates and $\boldsymbol{\Phi}_m$ is the modal matrix. As an example, the first two internal vibration modes of a 2D beam are shown in figure 2.

$$\mathbf{u} = \begin{bmatrix} \mathbf{u}_b \\ \mathbf{u}_i \end{bmatrix} = \boldsymbol{\Phi}_{CB} \begin{bmatrix} \mathbf{u}_b \\ \mathbf{q} \end{bmatrix} = \begin{bmatrix} \mathbf{1} & \mathbf{0} \\ \boldsymbol{\Psi} & \boldsymbol{\Phi}_m \end{bmatrix} = \boldsymbol{\Phi}_{CB} \begin{bmatrix} \mathbf{u}_b \\ \mathbf{q} \end{bmatrix}$$
(6)

The Craig-Bampton transformation matrix $\boldsymbol{\Phi}_{CB}$ can be used to reduce equation 5 to equation 7.

$$\boldsymbol{\Phi}_{CB}^T \mathbf{M} \boldsymbol{\Phi}_{CB} \begin{bmatrix} \ddot{\mathbf{u}}_b \\ \ddot{\mathbf{q}} \end{bmatrix} + \boldsymbol{\Phi}_{CB}^T \mathbf{C} \boldsymbol{\Phi}_{CB} \begin{bmatrix} \dot{\mathbf{u}}_b \\ \dot{\mathbf{q}} \end{bmatrix} + \boldsymbol{\Phi}_{CB}^T \mathbf{K} \boldsymbol{\Phi}_{CB} \begin{bmatrix} \mathbf{u}_b \\ \mathbf{q} \end{bmatrix} = \boldsymbol{\Phi}_{CB}^T \begin{bmatrix} \mathbf{P} \\ \mathbf{0} \end{bmatrix}$$
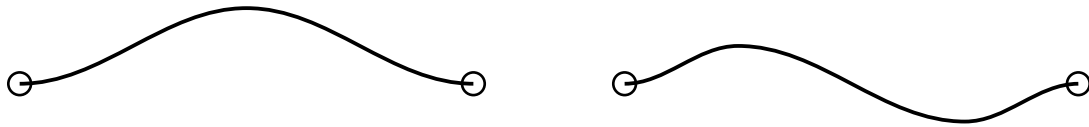(7)

Figure 2: First and second internal vibration modes of a 2D beam

1.1.3 Advantages of substructuring

Substructuring has several advantages compared to calculating the entire model at once [3]. Overall it can be stated that substructuring results in a more flexible and efficient modelling process.

- Structures which are too complex to be evaluated at once, can be divided into smaller, more simple parts;

- It is not necessary to re-evaluate the entire model if only one substructure is changed;

- Different people or project groups can work simultaneously on different substructures;

- Identical parts can be copied, which increases the evaluation speed.

1.2 Multibody dynamic analysis

A multibody dynamic analysis determines the motion of a system consisting of multiple bodies with large relative motions. This creates an understanding of the interaction between the moving parts, as well as with their environment. The parts are connected to each other using joints, which constrain the motion. This is described by constraint equations, which are often nonlinear for large motions. Large motions also add extra loads because of inertia effects, which are not taken into account in linear FE models.

An MBD analysis usually considers all parts to be rigid. However, flexibility of the parts can influence the motion, which makes the analysis inaccurate. To improve accuracy, flexibility should be implemented in the multibody dynamic model.

1.3 Thesis objective

In amusement ride manufacturing it is currently common practice to use extensive FE models to predict the deformation and internal stresses. However, the large motions in most rides lead to highly nonlinear equations of motion, which are not analytically solvable [4]. Multibody dynamic models are capable of analysing structures with large motions. However, these models typically assume the parts to be rigid and only basic parts can be made flexible. This research describes a method of combining FE and MBD to obtain a flexible model which can account for large motions.

This thesis focuses on a specific type of theme park rides, which can be described as "rotating tower rides". Several ride manufacturers build rides consisting of a rotating tower with a bearing at the bottom and some type of gondolas attached. Some examples are shown in figure 3: the Vertical Swing made by Zamperla, the Sky Roller by Gerstlauer, the High Swing by KMG, the Tower by SunKid and the FlyingWheels by Metallbau Emmeln. All these rides have in common that it is difficult to predict the loads and internal stresses accurately, especially at the connection of the tower to the base.

1.4 Thesis outline

The next section introduces the case study, including an explanation of the different models which are used in this thesis. A static analysis is used as verification for these models in section 3, which shows some issues in one of the models. Section 4 contains a dynamic analysis where large motions are constrained, which means that the results should be similar for all models. These results are compared with a total dynamic analysis including large motions in section 5. The conclusion is given in section 6, followed by recommendations for further research in section 7.

(a) Vertical Swing by Zamperla [5]

(b) Sky Roller by Gerstlauer [6]

(c) High Swing by KMG [7]

(d) Tower by SunKid [8]

Figure 3: Some examples of rotating tower rides

2 Case study

This thesis focuses on rotating tower rides, of which the Wirbelbaum is chosen as an example (figure 4). The Wirbelbaum is a ride of the type FlyingWheels by Metallbau Emmeln and located in Toverland, a Dutch theme park in Sevenum. It consists of a vertical tower, which rotates around its axis. Two gondolas are attached to either side of the tower, which move slowly up and down. Each gondola has three rotating arms, with on each arm a hanging cart. Guests can rotate the cart themselves, using a fixed steer in the middle of the cart. Figure 4b shows the SolidWorks model where the inner structure is clearly visible.

(a) Photo of the Wirbelbaum [9]
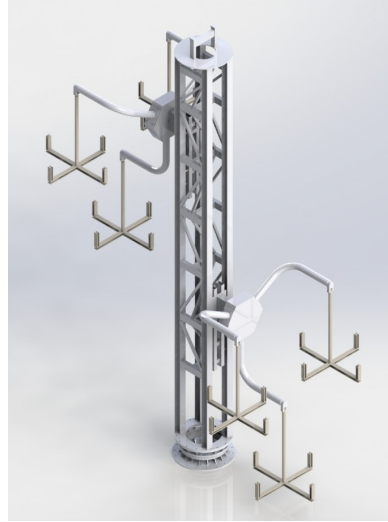
(b) Structure of the Wirbelbaum [10]

Figure 4: Overview of the structure

2.1 Critical point of the structure

The ride manufacturer designed the Wirbelbaum for infinite fatigue life using only hand calculations, which are added in appendix A. However, after 12 years of operation, cracks are discovered in welds at several locations at the bottom of the structure, where the tower is connected to the bearing [10]. Although these cracks have been repaired and reinforced, crack initiation did not stop and this part of the structure remains problematic. This shows the relevance of more realistic stress prediction at this location, which is why this is the main focus of this thesis.

In this case study the Wirbelbaum is divided into two structural parts: the tower and the bearing. The stresses and deformations in the structure of the gondolas are not taken into account.

2.2 Software

This research combines different FE and dynamic multibody software in order to compare the results. The detailed model in SolidWorks is obtained from previous research [10] and some adaptations are made (figure 4b). A flexible model of the tower consisting of beam elements is made in both Matlab and Ansys. A flexible model of the bearing is also made in Ansys. These results are used to obtain both a rigid and a flexible model of the tower and bearing in MSC Adams. A step-by-step overview of how to build the flexible multibody dynamic model is added in appendix B.

2.2.1 Matlab

The tower is modelled in Matlab, consisting entirely of beam elements. Figure 5 shows the model with the global coordinate system, where the origin is located at the center of the bottom of the tower. The carts would be attached at the y,z-planes of the tower.

The model is built by manually implementing stiffness and mass matrices for slender beam elements. These are defined in a local coordinate system and therefore must be rotated to the global coordinate system. A
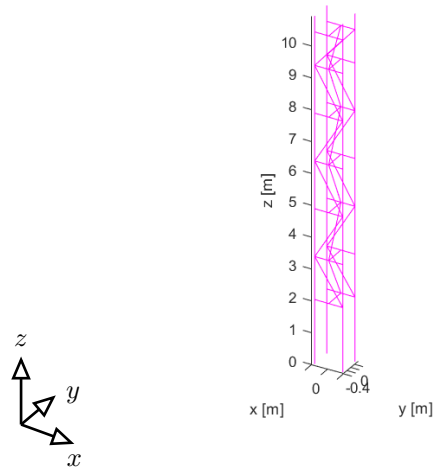
Figure 5: Matlab model of the tower

Boolean matrix is used to couple the elements and obtain the stiffness and mass matrices of the complete tower. An elaborate description of the Matlab model can be found in appendix C.

Matlab is also used for data processing and to visualise results.

2.2.2 Ansys

Both the tower and the bearing are modelled separately in Ansys Mechanical APDL. The tower consists of beam elements and looks similar to the Matlab model, as can be seen in figure 6a.

Most of the bearing is meshed with SOLID187 elements. However, the flat plates in between the upper and lower ring have a very small thickness compared to their other dimensions. Using 3D solid elements with small thickness leads to problems of shear locking and ill-conditioning. While these problems can be solved by using more elements, it would lead to an excessive amount of dofs [2]. Therefore these parts are meshed with SHELL281 elements. The meshed bearing is shown in figure 6b.

Modal neutral files (.mnf) have been made of both parts to enable flexibility in the Adams model. This process creates a reduced model of the structure, and for this purpose several interface nodes must be defined. Interface nodes are mandatory at the location of boundary nodes and nodes where an external force is applied.

The tower is connected to the bearing with four points at the bottom. These nodes should therefore be interface nodes, but this rigid connection leads to overconstraints and therefore possibly an inaccurate model. Therefore, these four nodes are reduced to a single one in the middle using a rigid region, which means that these nodes are not allowed to deform with respect to each other. The nodes at the top of the tower are also considered interface nodes, to obtain a more accurate description of the structure. The nodes where the load is applied are the last interface nodes.
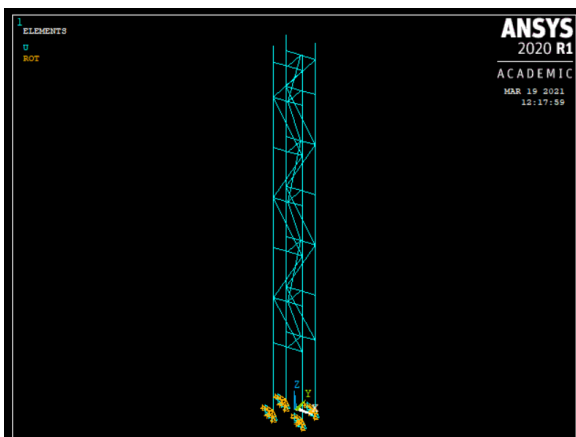
(a) Tower in beam elements
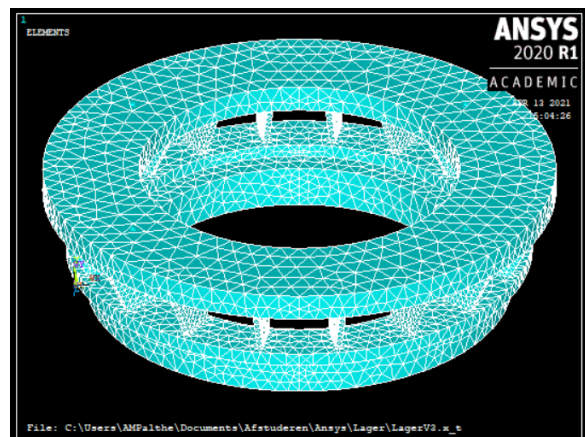
(b) Bearing in solid and shell elements

Figure 6: Ansys models

10

2.2.3 Adams

The tower is also modelled in MSC Adams, for Automatic Dynamic Analysis of Mechanical Systems. Adams is used for multibody simulations, but a modal neutral file (.mnf) is necessary to change a body from rigid to flexible. This results in a reduced model. The rigid model, including the carts and gondolas, is shown in figure 7a. This model is used to determine the loads on the tower during the ride. Figure 7b shows the multibody model with a flexible tower.

It can be seen that Adams uses a different coordinate system, where the vertical axis is the y-axis. All data in this thesis obtained from Adams is transformed to the coordinate system shown in the Matlab model in figure 5, where the vertical axis is the z-axis.

(a) Rigid model including gondolas   (b) Multibody model with flexible tower
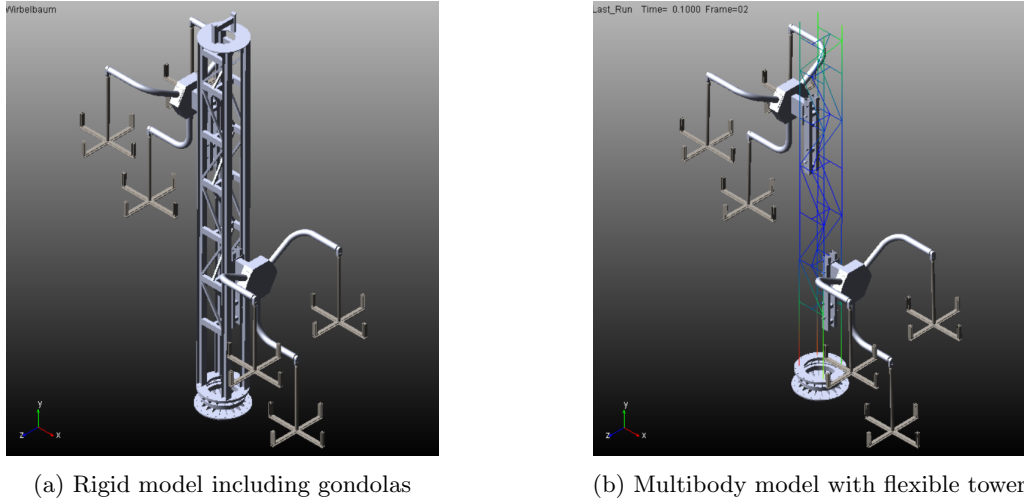
Figure 7: Adams models

2.3 Ride programme

The ride is simulated in Adams using STEP5 functions and based on previous research using the Wirbelbaum as case study [10]. The main advantage of STEP5 functions over regular STEP functions is that it has smooth transitions and thus a continuous second derivative.

While one gondola is at the bottom to give guests the chance to enter, the other gondola is rotating at the top of the tower with a constant rotational velocity of 5 RPM. After loading all carts of the gondola, both gondolas move vertically to the middle of the tower with a maximum translational velocity of 0,5 m/s, while they act as each others counterweights. Simultaneously the tower starts to rotate in clockwise direction with a rotational velocity of 6 RPM. After two and a half rotation, the other gondola moves down to switch guests, while the other moves upward.

Figure 8 shows a graphical representation of the translation and rotation of the gondolas during the ride.

(a) Translation of the gondolas   (b) Rotation of the gondolas
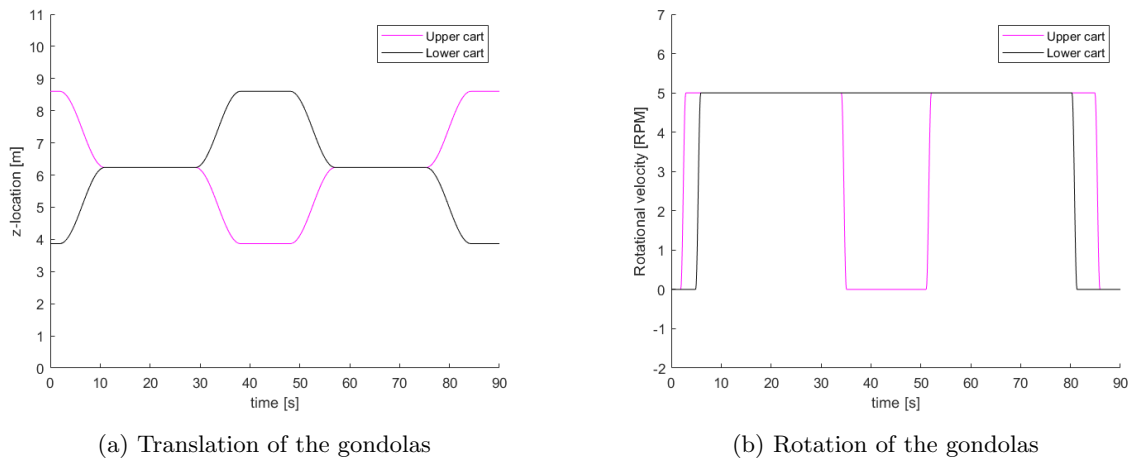
Figure 8: Ride programme

2.3.1 Loads on tower

The loads exerted by the carts on the tower during the ride programme are determined. For this purpose, gravity is applied and each gondola is loaded with a force of 1500 N in negative z-direction, to mimic the presence of guests. The carts are attached to the tower with four sliding interfaces as shown in figure 9. The coordinate system shown is local and fixed to the cart, and will therefore rotate when the tower rotates. However, to prevent overconstraints, the carts in the model are connected only at the upper left joint.
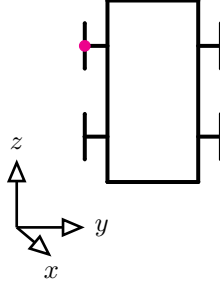
Figure 9: Cart including local coordinate system and the location of the active joint (in pink)

The loads exerted by the carts on the tower as a function of time are shown in the local coordinate system in figure 10. The upper cart represents the cart starting at the top during simulation. The force in x-direction is zero when the tower is stationary and has a nearly constant value of 1100 N when the tower is rotating. This force is caused by the centrifugal acceleration.

The force in y-direction, which is pointed in the direction of the rotation, is only non-zero during the acceleration and deceleration of the rotation of the tower.

The force in z-direction is zero for all t. This is caused by the translational joint, which does not constrain the z-direction and can therefore not produce a reaction force in that direction. This corresponds to the real life situation, where the translational motion is also not driven at the cart. The two carts are connected to each other by a cable, which is connected by a pulley to the top of the tower. However, since in this thesis the comparison of the different models is the most important, this force due to gravity is added at the location of the joint.

The moment around the x-axis before movement has a constant value of approximately -5100 Nm. This corresponds with the force in z-direction multiplied with half the width of the cart, which is the distance to the force. The rotating movement of the gondolas adds a constant value to this moment. Only the upper cart shows some disturbance at $30 \leq t \leq 55s$, because this cart stops rotating during that time, which causes deceleration and acceleration.

The moment around the y-axis is large, because of the large distance to the center of mass. The centrifugal acceleration due to rotation of the tower decreases this moment slightly.

The moment around the z-axis is mostly zero, with small deviations during acceleration and deceleration of the rotation of the tower.

Figure 10: Forces on the tower in the local coordinate systems of the carts, obtained from Adams

3 Static analysis

A static evaluation is used to determine if the models are valid. Both the deformation at the top and the reaction forces at the bottom of the tower due to a static load are determined and compared. The static load consists of a force of 10 MN in negative z-direction and a moment of 10 MNm around the y-axis, and is visualised in figure 11 (including the numbering of the top nodes). Gravity is left out for better comparison between the models.
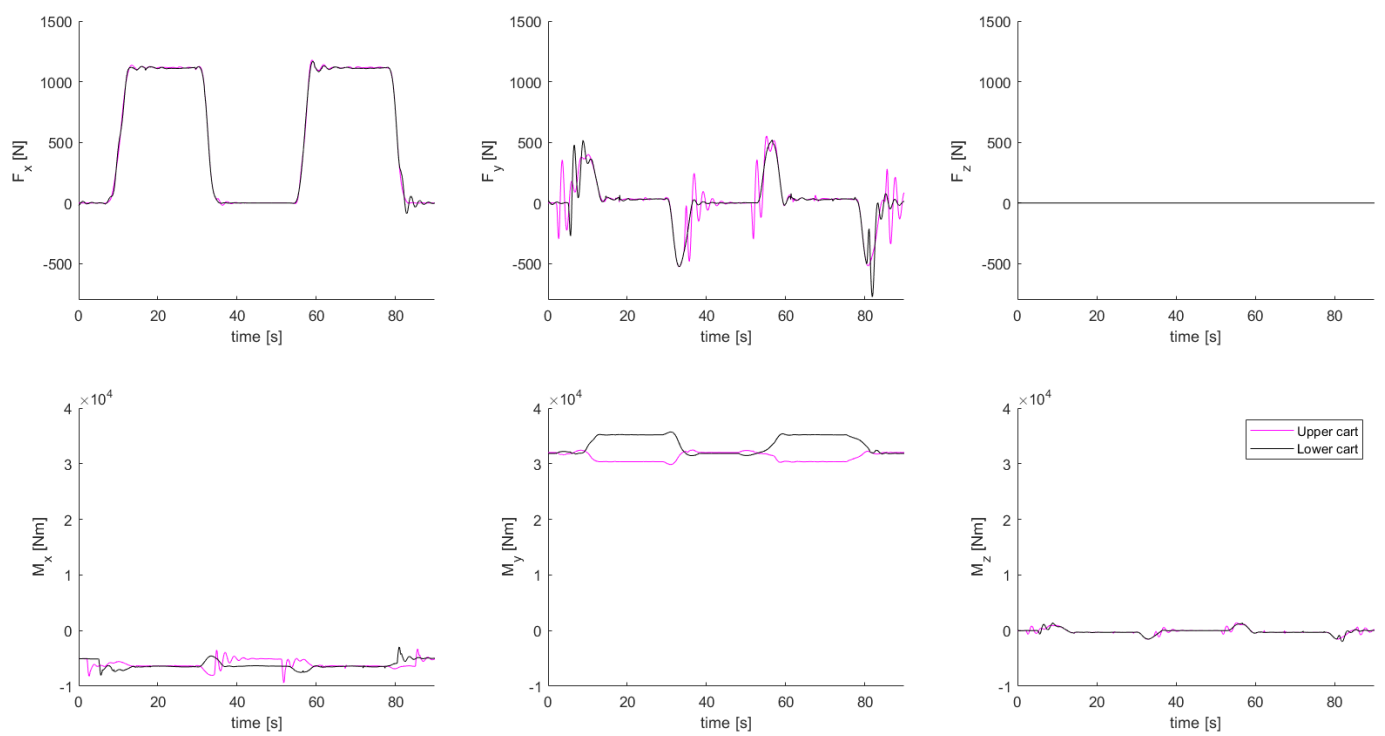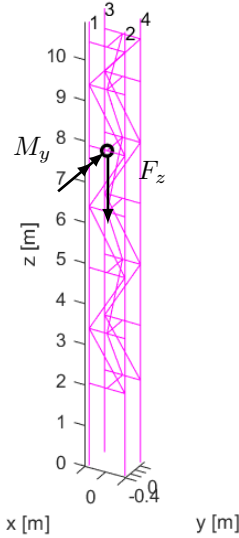

Figure 11: Visualisation of the static load case

3.1 Deformation

The static deformation of the four nodes at the top of the tower is determined using all models. Figure 12 shows the result using the manually entered stiffness and mass matrices and using the matrices obtained from Ansys. It can be seen that the deformation looks realistic and that the results of the manually entered matrices are very similar to those using the matrices obtained from Ansys.

The displacement of the four nodes at the top of the tower after deformation are listed in table 1. First of all, the analysis in Ansys itself gives the exact same result as the analysis in Matlab using the stiffness and mass matrices from Ansys. This indicates that the calculation method in Matlab is correct.

The small difference between the Matlab and Ansys model is mostly along the x-direction, which in this situation would be caused by bending due to the applied moment. This difference is probably caused by assuming slender beam elements in the Matlab model, which means that shear is neglected. This assumption and resulting simplification are explained in appendix C. The smallest aspect ratio occurring in this model is 5, which means that for these beams shear should not be neglected and Timoshenko beam theory should be applied.

The same load is applied on the model of the tower in Adams, where one of the models uses a single joint at the centre of the bottom of the tower to avoid residual stress due to non-alignment. The displacement of the four nodes at the top is also added in table 1. It can be seen that the deformations calculated in Adams are considerably different. The deformed tower is shown from above in figure 13, the node where the load is applied is at the bottom in this figure. It can be seen that the Adams model shows more resistance to rotational deformation and the Matlab model is the only one showing some warping. Since the data for this model is imported from Ansys, the difference should originate at the exportation to Adams or in the calculation in Adams itself. The problems in the Ansys-Adams interface are elaborated in appendix D.

3.2 Reaction forces

The reaction forces and moments in the bottom four nodes are determined in the same static analysis. Verification can be done by considering equilibrium. Since gravity is left out in all models, the sum of the reaction forces and the combined reaction moment in the four bottom nodes should equal the applied load. The combined reaction moments are determined using equation 8.

14
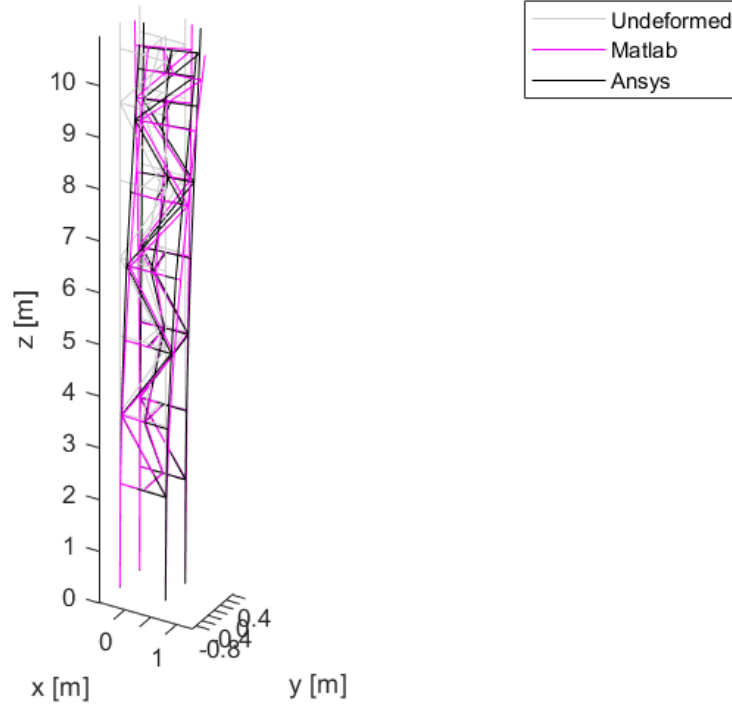
Figure 12: Static deformation

Table 1: Deformation of the top four nodes [m]

	Ansys			Ansys matrices			Matlab			Adams single joint			Adams 4 joints		
n	x	y	z	x	y	z	x	y	z	x	y	z	x	y	z
1	0,66	-0,50	0,02	0,66	-0,50	0,02	0,83	-0,48	0,03	0,61	-0,60	0,01	0,65	-0,58	0,01
2	0,66	-0,11	-0,07	0,66	-0,11	-0,07	0,83	-0,11	-0,09	0,61	-0,60	-0,07	0,65	-0,58	-0,07
3	0,37	-0,50	0,02	0,37	-0,50	0,02	0,19	-0,49	0,01	0,60	-0,61	0,04	0,64	-0,58	0,04
4	0,36	-0,11	-0,02	0,36	-0,11	-0,02	0,19	-0,10	-0,01	0,61	-0,60	-0,03	0,64	-0,58	-0,03

$$\Sigma M_x = \Sigma M_{x,nodes} + \Sigma F_z dy$$
$$\Sigma M_y = \Sigma M_{y,nodes} + \Sigma F_z dx \tag{8}$$
$$\Sigma M_z = \Sigma M_{z,nodes} + \Sigma F_x dy + \Sigma F_y dx$$

The results for the different models are shown in table 2.

It can be seen that the results for the reaction forces are very accurate. The reaction moments, however, deviate. The reaction moment M_y should oppose the applied moment of 10 MNm. The applied load in negative z-direction should produce a reaction moment M_x of $-10 \cdot 0,33 = 3,3$ MNm. The reaction moment M_z should be zero.

It can be seen that the reaction moments obtained from Adams are larger. The difference in the moment around the x-axis is largely caused by the difference in deformation along the y-axis, which changes the distance between the applied load and the joint. The overconstraints in the 4-node Adams model lead to higher forces and moments at the four joints.

3.3   Conclusion of the verification

Extra research is dedicated to the problems in the Ansys-Adams interface and added in appendix D. The results in this appendix clearly show the linearity of the FE models and how the results of the different models converge for smaller loads and thus smaller deformations. For larger deformations Adams is expected to give better results, since it takes nonlinear effects into account.

Unfortunately, it proved infeasible to solve the problem in the Wirbelbaum model. The remainder of this thesis discusses the method of flexible multibody analysis without providing accurate numerical results.
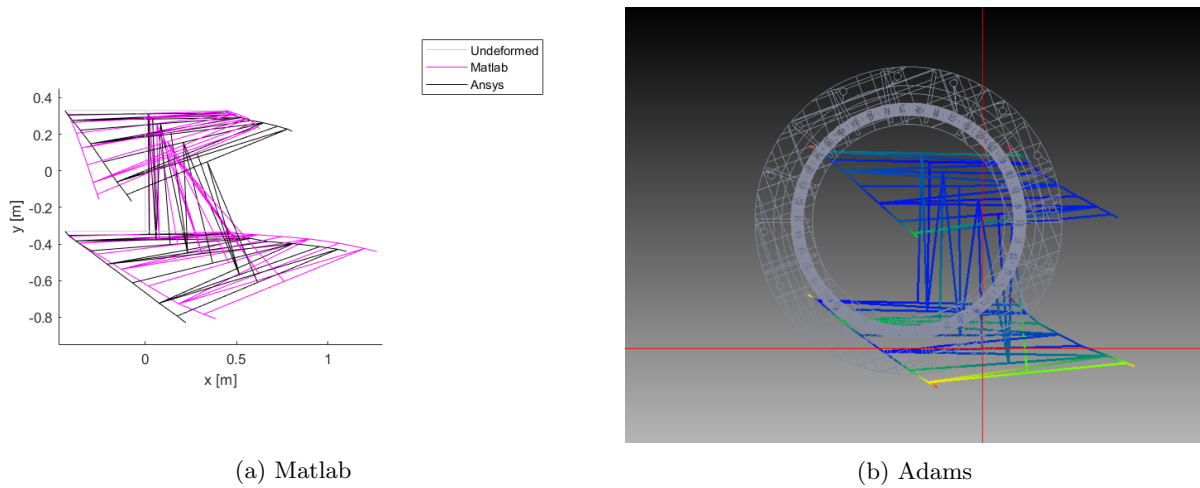
(a) Matlab

(b) Adams

Figure 13: Deformed tower seen from above

Table 2: Reaction forces [MN] and moments [MNm]

	Ansys	Ansys matrices	Matlab	Adams single joint	Adams 4 joints
ΣF_x	0	0	0	0	0
ΣF_y	0	0	0	0	0
ΣF_z	10	10	10	10	10
ΣM_x	-3,3	-3,3	-3,3	7,3	7,2
ΣM_y	-10	-10	-10	-13	-14
ΣM_z	0	0	0,10	0	0,01

4 Dynamic analysis of stationary tower

In this section the tower is considered stationary and constrained in all directions at the bottom, because eliminating this large motion should lead to similar results from the different models. The carts and the gondolas move according to the ride program as shown in figure 8. The resulting loads on the tower are shown in figure 14, again in the local coordinate systems of the carts.
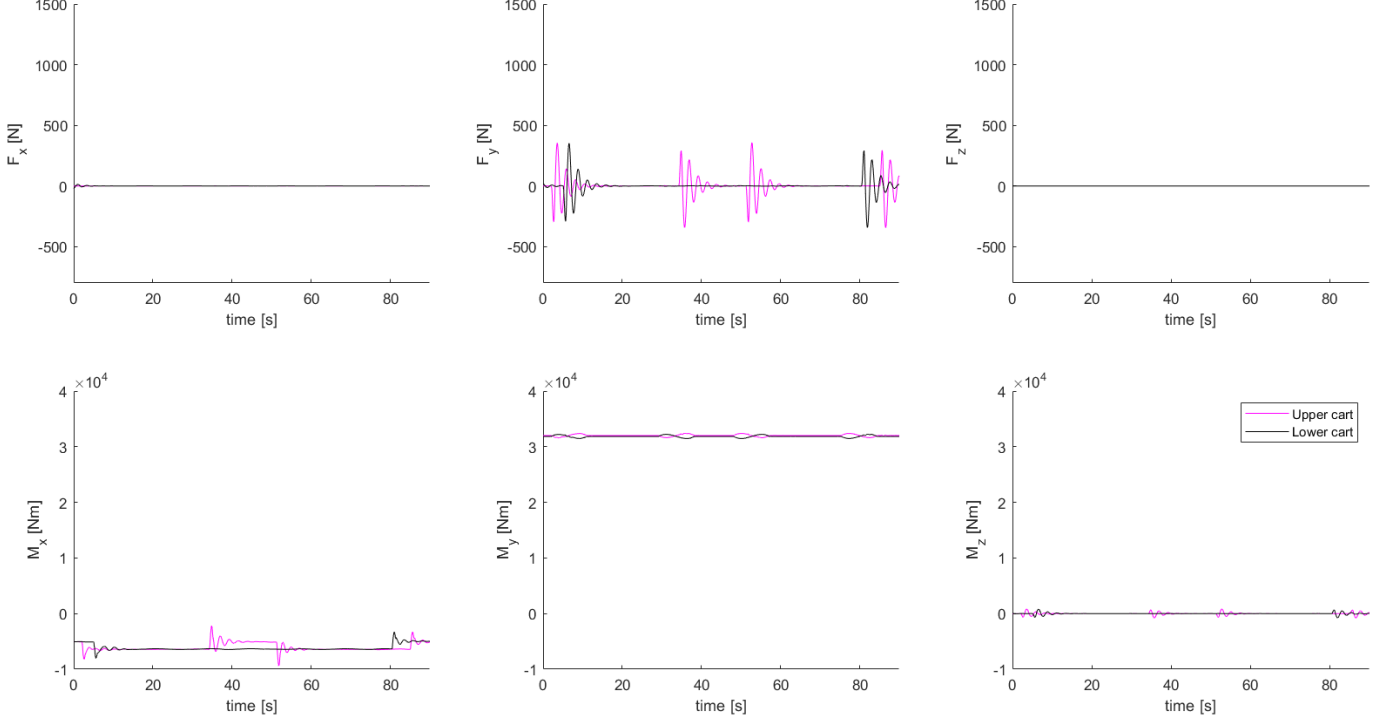
Figure 14: Forces on the tower without rotation obtained from Adams

4.1 Equivalent load

The load exerted by the gondolas moves continuously up and down the tower. However, nodes are only located at the joints. Therefore the load is transformed into equivalent loads on the nearest nodes for all time steps. This can be done by multiplying the original load vector of size 6x1 with matrix $\mathbf{A}$ containing shape functions (equation 9). In this matrix $\xi = \frac{x}{L}$, which is the dimensionless location along the beam of the original load. The result is an equivalent load vector of size 12x1, containing all three forces and moments on the two closest nodes. A detailed derivation of this transformation is described in appendix E.

$$\mathbf{P}_{eq} = \mathbf{AP} = \begin{bmatrix} 1-\xi & 0 & 0 & 0 & 0 & 0 \\ 0 & 1-3\xi^2+2\xi^3 & 0 & 0 & 0 & -\frac{1}{L}(6\xi-6\xi^2) \\ 0 & 0 & 1-3\xi^2+2\xi^3 & 0 & -\frac{1}{L}(6\xi-6\xi^2) & 0 \\ 0 & 0 & 0 & 1-\xi & 0 & 0 \\ 0 & 0 & L(\xi-2\xi^2+\xi^3) & 0 & 1-4\xi+3\xi^2 & 0 \\ 0 & L(\xi-2\xi^2+\xi^3) & 0 & 0 & 0 & 1-4\xi+3\xi^2 \\ \xi & 0 & 0 & 0 & 0 & 0 \\ 0 & 3\xi^2-2\xi^3 & 0 & 0 & 0 & \frac{1}{L}(6\xi-6\xi^2) \\ 0 & 0 & 3\xi^2-2\xi^3 & 0 & \frac{1}{L}(6\xi-6\xi^2) & 0 \\ 0 & 0 & 0 & \xi & 0 & 0 \\ 0 & 0 & L(-\xi^2+\xi^3) & 0 & -2\xi+3\xi^2 & 0 \\ 0 & L(-\xi^2+\xi^3) & 0 & 0 & 0 & -2\xi+3\xi^2 \end{bmatrix} \begin{bmatrix} F_x \\ F_y \\ F_z \\ M_x \\ M_y \\ M_z \end{bmatrix} \quad (9)$$

Because the exerted load is moving, ξ is a function of time and the two closest nodes change through time.

4.2 Quasi-static evaluation

A quasi-static evaluation is performed first, such that the results can later be compared to the dynamic evaluation. In a quasi-static evaluation, all dynamic effects are left out, which reduces the equation of motion to equation 10.

$$\mathbf{K}\mathbf{u} = \mathbf{P} \tag{10}$$

This equation is simply repeated for each time step. Its simplicity makes it a good accuracy measure for more complicated dynamic calculations.

4.3 Dynamic evaluation

The Newmark-β integration scheme is used to determine the displacement, velocity and acceleration of all the nodes at each time step. This integration scheme is implicit (except when $\beta = 0$), which means that the current displacements are related to current accelerations, as well as responses from previous time steps. The main advantage of implicit integration schemes is their unconditional stability, though explicit methods are more computationally efficient.

Every dynamic system can be described by its equation of motion, of which the standard form is shown in equation 11.

$$\mathbf{M}\ddot{\mathbf{u}} + \mathbf{C}\dot{\mathbf{u}} + \mathbf{K}\mathbf{u} = \mathbf{P} \tag{11}$$

Using the Newmark-β integration scheme it is possible to obtain equations for the displacement, velocity and acceleration at the next time step as a function of the previous time step. These equations and their derivations are explained in appendix F.

4.4 Deformation

The deformation of the four top nodes is determined using both the Matlab model and the Adams model. The results obtained from Matlab are shown in figure 15a. The coloured graphs show the results according to the dynamic analysis, the black graphs of the Matlab model are determined with the quasi-static analysis. It can be seen that those results are similar, apart from the vibrations added in the dynamic analysis.

(a) Matlab model
(b) Adams model
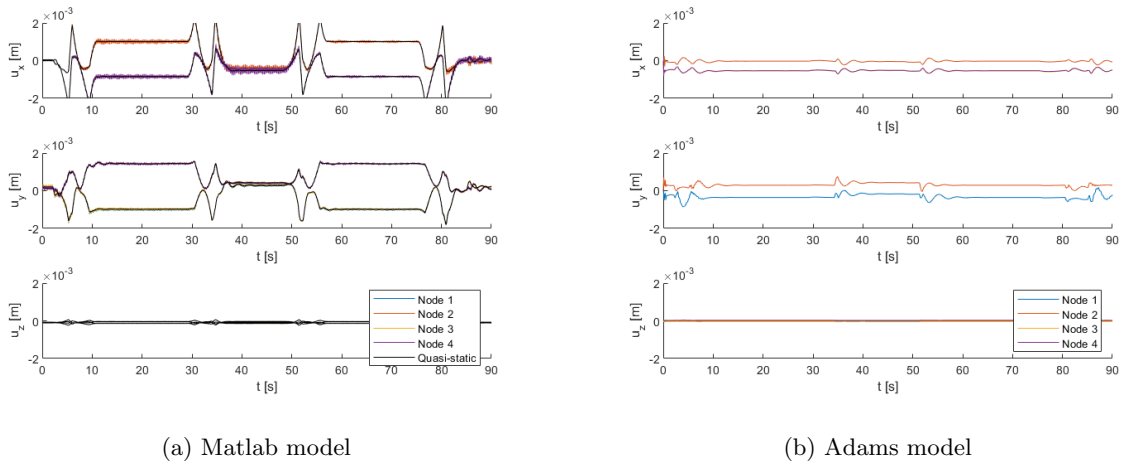
Figure 15: Deformation of the four top nodes when the tower does not rotate

Figure 15b shows that the deformations according to the Adams model has the same order of magnitude as those according to the Matlab model, but otherwise the results are quite different. At $10 \leq t \leq 30$ for example, the two carts are at the same height and rotating at constant velocity. During this time the Matlab model is rotated around the z-axis, while the cross section remains similar. The Adams model again shows more resistance to rotational deformation, similar to the static deformation in section 3.1.

4.5 Reaction forces

The reaction forces and moments at the bottom of the tower are shown in figure 16. Figure 16b shows the data as directly measured in Adams, where the tower is connected to the bearing with one joint in the center.

The reaction forces in Matlab are determined based on the calculated deformations and equation 11. The results of the four nodes at the bottom of the tower are combined to obtain the reaction forces and moments as if the tower would only be connected through a single point in the middle. The result of the dynamic calculation is shown in pink in figure 16a, the quasi-static results are shown in black.

Since there are no applied forces in x- and y-direction, the reaction forces in these directions should be zero. It can be seen that this is true for both models, only during acceleration and deceleration a reaction force in y-direction is shown. The force in z-direction is constantly 82,3 kN for both models, which equals the combined mass of the tower and gondolas plus the forces applied at the gondolas.

The moment around the x-axis is mostly zero. This is because the moments due to the rotating gondolas are equal and opposite. A reaction moment does arise between $34 \leq t \leq 52$ s, because this is where one of the gondolas stops rotating.

Note the different axes for the moment around the y-axis. For the Adams model the reaction moment fluctuates around zero, which is again due to equal forces from the gondolas. However, this is not true for the Matlab model. Especially at $34 \leq t \leq 52$ s there is a large reaction moment. During this time, one of the gondolas is located at the bottom of the tower, while the other is at the top. This causes bending in the tower, which increases this moment.

The moment around the z-axis again fluctuates around zero, because no forces in x- or y-directions or a moment around the z-axis is applied.

4.6   Internal stress

The internal stresses of each element of the tower calculated in Matlab are shown in figure 17. This figure only shows the quasi-static results, to improve clarity. The highest normal stresses occur in elements 44 and 75 during constant rotation of the gondolas. This is not surprising, since this is the location where the gondolas are during that time.

The highest shear stress at $11 \leq t \leq 29$ is in element 75, which is one of the horizontal elements where the gondolas are located during that time. High peaks are seen in elements 40 and 48 when the gondolas move up and down. These elements are again the horizontal elements where the gondolas are located during that time. All of the high shear stresses are located in the shortest elements of the structure.

4.7   Eigenfrequencies and eigenmodes

The eigenvalues and eigenvectors of the stiffness and mass matrices are calculated in order to determine the eigenfrequencies and eigenmodes of the structure. The first six eigenmodes obtained from Matlab are visualised in figure 18, including the corresponding frequencies.

Since the construction is very large and heavy, it is expected that the first eigenfrequencies are very low. The excitation frequencies in the ride program are in the order of 1 Hz, which is well below the first eigenfrequency.
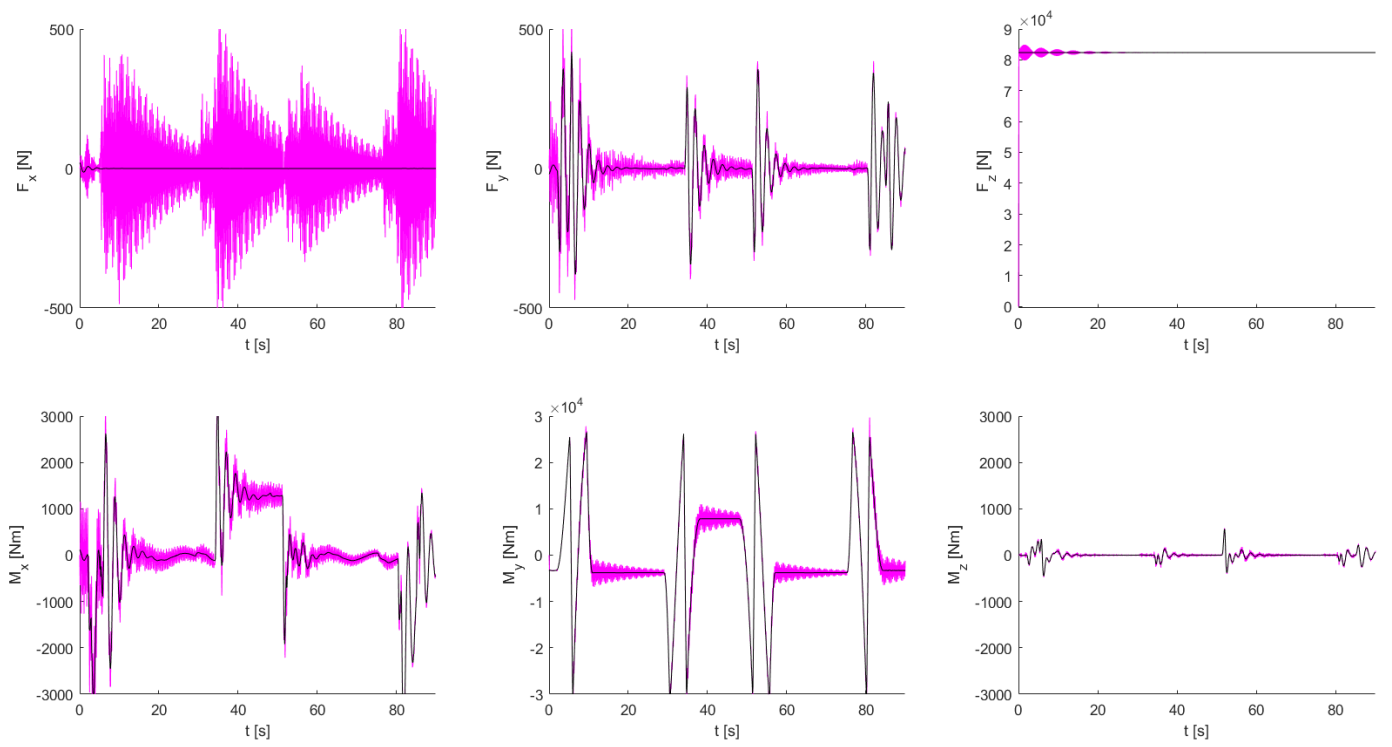
(a) Matlab model, quasi-static results in black
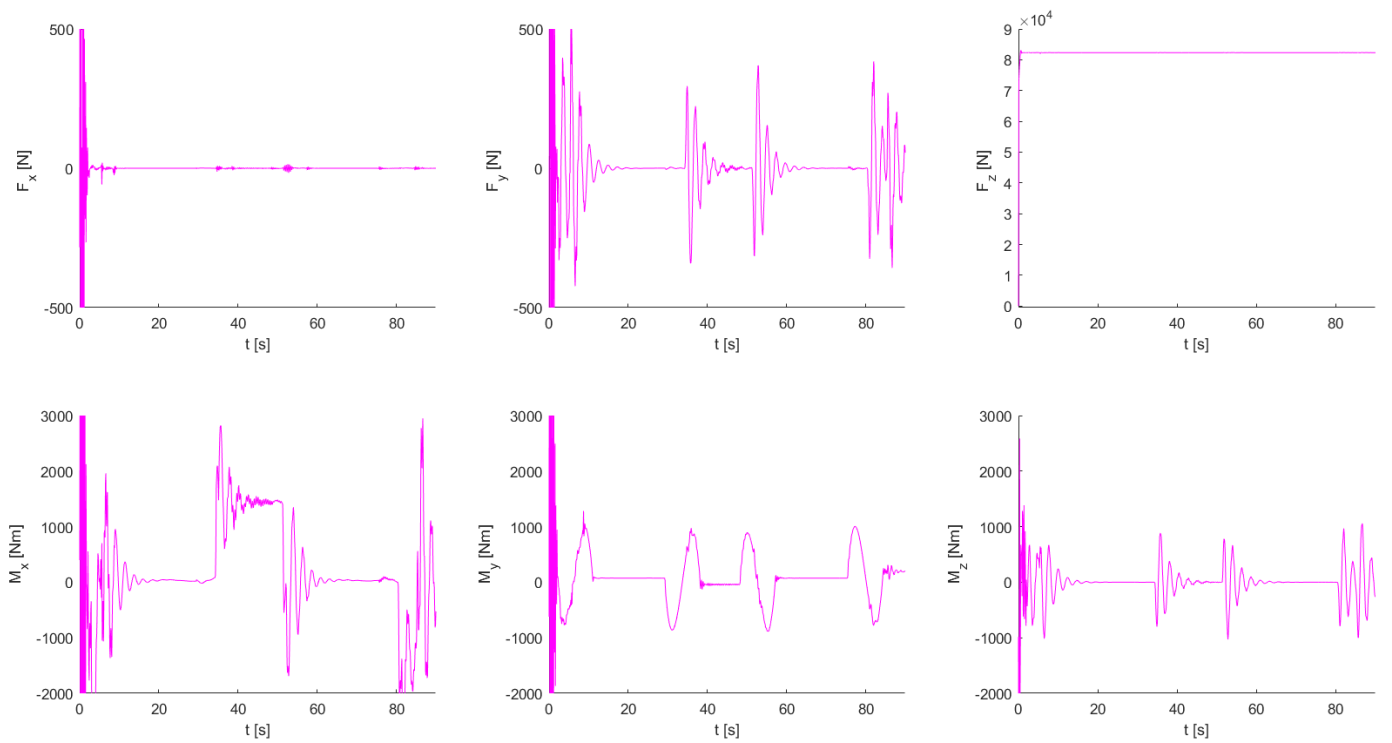
(b) Adams model

Figure 16: Reaction forces at the bottom of the tower
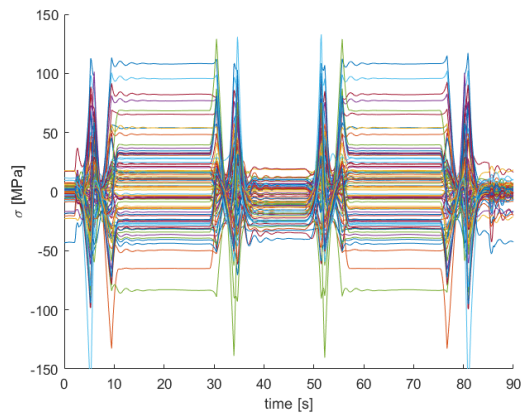
(a) Normal stress
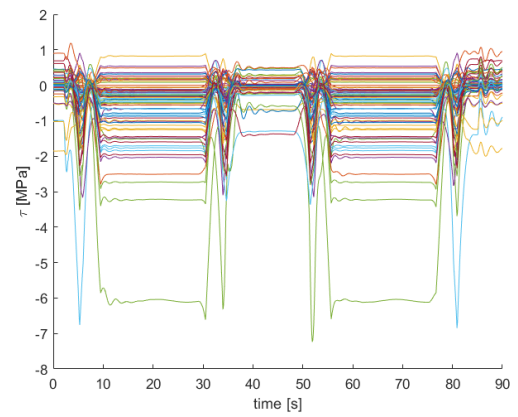
(b) Shear stress

Figure 17: Internal stresses of the tower (quasi-static)
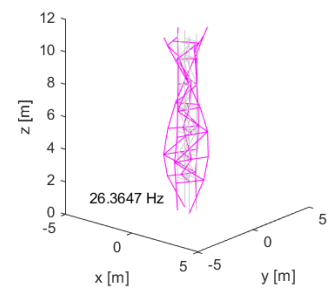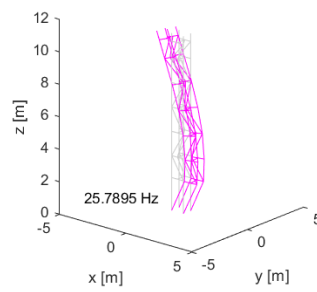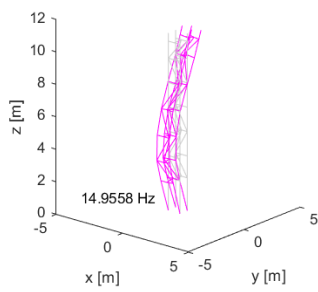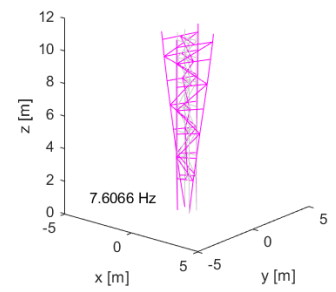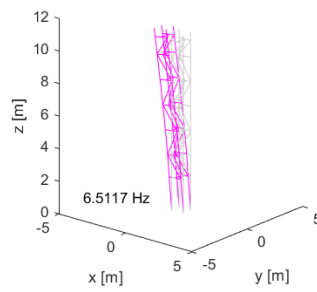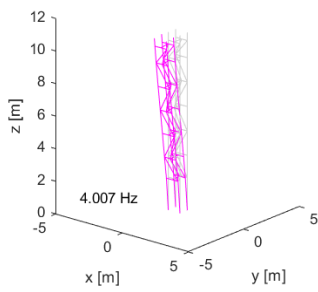
Figure 18: Eigenmodes of the tower determined in Matlab

5 Analysis of the rotating tower

In this section the tower is rotating conform its ride programme as described in section 2.3. Only results from the Adams model are shown, since this is the only model capable of handling this large motion. These results are compared to those of the stationary tower in section 4 to determine the effect of large rotation on the structure.

5.1 Deformation

The deformation of the four top nodes is determined in the local coordinate system, which is fixed to the tower during rotation. The result is shown in figure 19, which includes the deformation without rotation for comparison (as seen before in figure 15b). It is clear to see that adding the rotation of the tower increases the deformation significantly and that the peaks have increased.

It is odd however that the mean deformation is so different. At $34 \leq t \leq 52$ s and $t = 90$ s the tower is not rotating, which means that the deformation should be the same.

(a) Without rotation   (b) With rotation
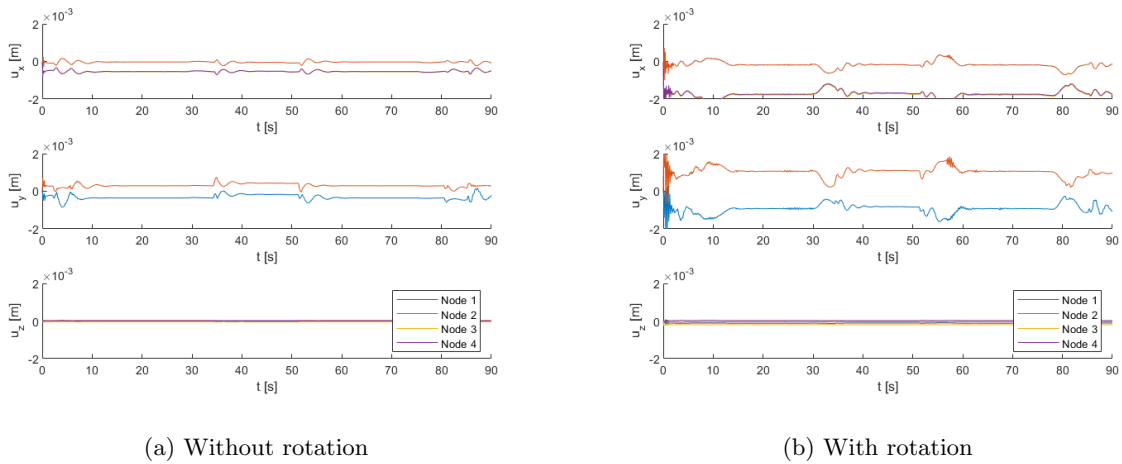
Figure 19: Deformation of the four top nodes with and without rotation

5.2 Reaction forces

The reaction forces and moments at the bottom of the tower during the ride are shown in figure 20. Comparing these to the forces without rotation in figure 16b shows the added loads due to this motion. Especially the moment around the z-axis shows high peaks at the rotational accelerations and decelerations, but the other graphs also show added vibrations at these times.

5.3 Conclusion

The increase in both deformation and reaction forces due to the large motion shows the need for dynamic multibody analysis. However, the difference in deformation at times when the tower does not rotate shows that this model contains inaccuracies.
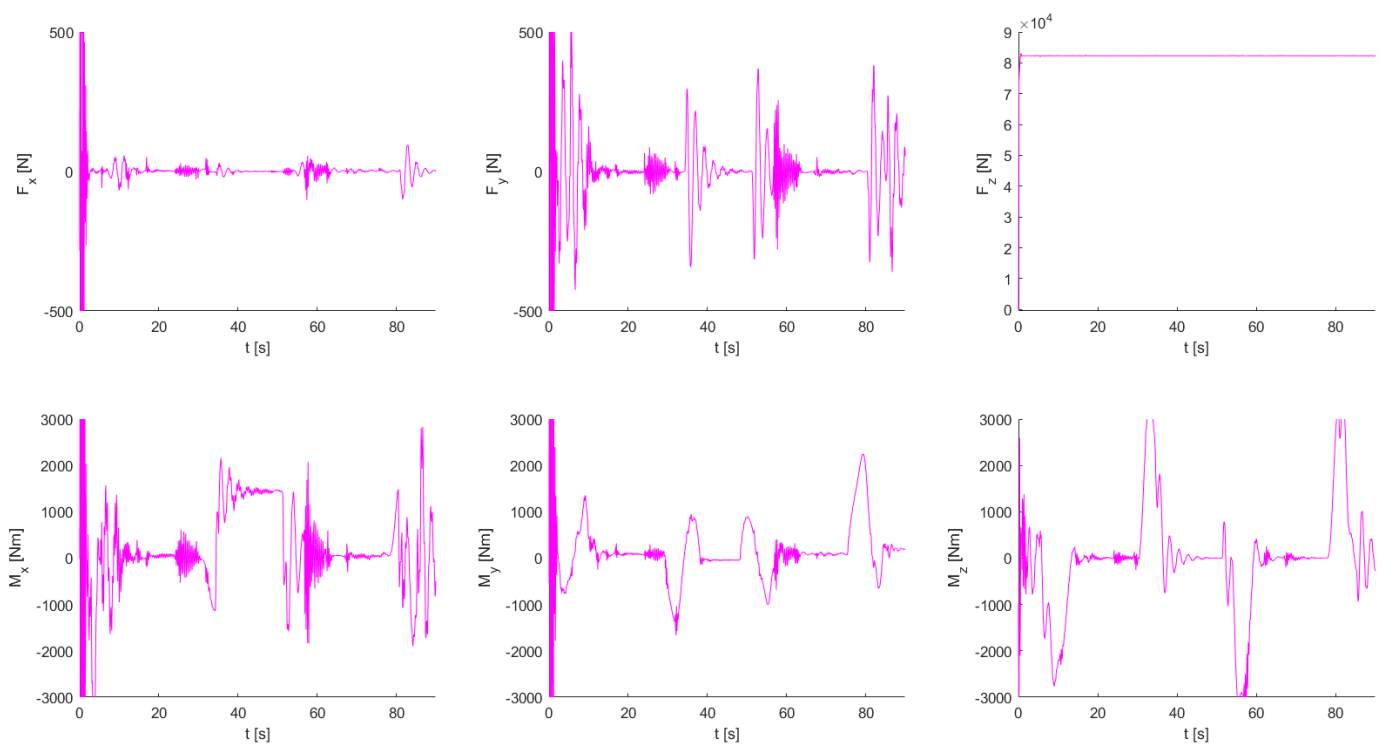
Figure 20: Reaction forces at the bottom of the tower during the full ride program

6   Conclusion

This thesis shows a method for implementing flexibility in a multibody dynamic model using a finite element model. MSC Adams is used as multibody dynamic software and Ansys is used to provide input for the flexibility of the part of interest. The advantage of this type of analysis is that the effects of a large motion are taken into account and that the results are valid for large deformations, as opposed to linear FE models.

A static analysis is used to validate the model. However, validating the flexible multibody dynamic model proved difficult. A short intermezzo proves the validity of this method for simpler models, such as a simple beam and structure. The results show the linearity of the FE models, which is why all models converge to the same results for small deformations. For large deformations, it is expected that the nonlinear Adams model is more accurate.

A dynamic analysis where the tower remains stationary is performed both in Adams and in Matlab. Since the load moves up and down the tower, it is not always applied at the location of a node. To accurately account for this load when it is located in between two nodes, it has to be transformed into an equivalent load acting on the closest nodes. This can be done by multiplication with a matrix of shape functions.

A dynamic analysis using the total ride program is performed only in Adams, since this is the only model which can account for the rotation of the tower. The results of the Adams model with and without rotation of the tower are compared to determine the added value of multibody dynamic analysis. The increase in reaction forces at the bottom of the tower due to this motion proves the need for this type of analysis.

It is expected that, if the problems occurring in this case study could be solved, the flexible multibody dynamic model described in this thesis would be able to accurately predict the stresses in complicated structures with large motions.

7 Recommendations

This thesis has shown on several points that the flexible multibody dynamic model of the Wirbelbaum in Adams contains an error, which does not appear in simple models built using the same method. More research is necessary to locate and solve this error.

This research focused on the tower, while cracks also occurred in the bearing. A model has been made in Ansys, but this data is not exported to Adams to make this part flexible as well. Redoing this analysis with both the tower and the bearing as flexible parts would further increase the knowledge on the loads and deformations occurring in the structure.

Some major simplifications are done in modelling the Wirbelbaum. These are used consistently in each model and therefore have no influence on the comparison between the different models, but do cause the results to deviate from reality. Therefore this should be improved if further research will consider the Wirbelbaum.

To make the use of flexible multibody dynamic analysis more common, it would be beneficial to simplify the method and implement the functionality in a single software package.

References

[1] K. K. Gupta and J. L. Meek. A brief history of the beginning of the finite element method. *International Journal for Numerical Methods in Engineering*, 39(22):3761–3774, 1996.

[2] Robert Cook, David Malkus, Michael Plesha, and Robert Witt. *Concepts and applications of finite element analysis, fourth edition.* Wiley India Pvt. Limited, 2007.

[3] S.N. Voormeren. *Dynamic substructuring methodologies for integrated dynamic analysis of wind turbines.* PhD thesis, TU Delft, 2012.

[4] J.P. Schilder. *Reader for Dynamics & Control.* University of Twente, September 2015.

[5] Zamperla. Vertical swing. `https://www.zamperla.com/products/vertical-swing/`. Accessed: 22-03-2021.

[6] Gerstlauer. Sky roller. `https://www.gerstlauer-rides.de/products/flat-rides/sky-roller-en-US/`. Accessed: 22-03-2021.

[7] KMG. High swing. `https://kmgrides.com/nl/rides/high-swing-nl/`. Accessed: 22-03-2021.

[8] SunKid. Tower. `https://www.sunkidworld.com/en/family-rides-tower`. Accessed: 22-03-2021.

[9] Arno Krol. Street view image of the wirbelbaum. `https://goo.gl/maps/kKMEmfiqVC63KxE27`, 2019. Accessed: 13-01-2021.

[10] L.S. Keizers. Structural fatigue analysis using flexible multibody dynamics. Master's thesis, University of Twente, May 2020.

[11] J.S. Przemieniecki. *Theory of Matrix Structural Analysis.* McGraw-Hill, 1968.

[12] A.M. Palthe. Structural anaysis afterburner. Applied Mechanics - Capita Selecta, February 2020.

[13] Ansys inc. Ansys APDL help. `https://ansyshelp.ansys.com/`, 2020. Accessed: 05-10-2020.

[14] Michael G. Katona, Robert Thompson, and Jim Smith. *Efficiency study of implicit and explicit time integration operators for finite element applications.* Civil Engineering Laboratory, 1977.

[15] Henri P. Gavin. *Numerical Integration in Structural Dynamics.* 2018.

A   Fatigue analysis of the Wirbelbaum
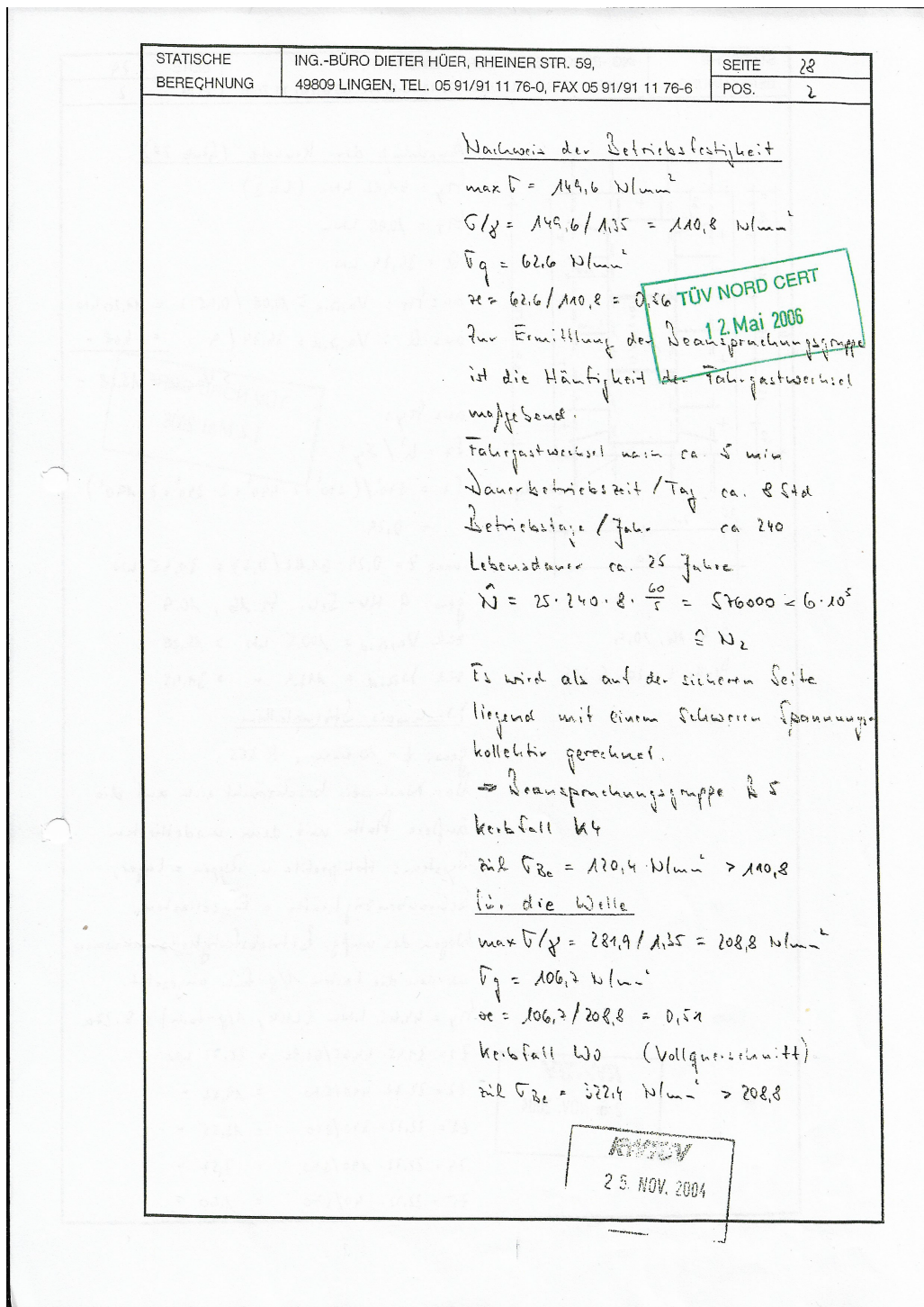
Figure 21: Fatigue analysis of the Wirbelbaum as performed by Metallbau Emmeln [10]

B Building a flexible multibody dynamic model

Several software packages are used to obtain the flexible multibody dynamic model. Figure 22 shows a flowchart of all the steps that need to be taken to build this model.

Figure 22: Flowchart showing the steps to build a flexible multibody dynamic model

C   Matlab model

The tower is modelled in Matlab and consists entirely of beam elements. Figure 23 shows the model, where the carts would be attached at the y-planes of the tower and the origin is located at the middle of the bottom of the tower. This appendix explains how this model is built.

Figure 23: Matlab model of the tower

C.1   Local stiffness and mass matrices

The starting point of this model is the local stiffness matrix. This matrix defines the stiffness of a beam element in its local coordinate system, where the origin is located at one of the nodes and the x-axis is positioned along the beam (figure 24). The local stiffness matrix based on Timoshenko beam theory is shown in equation 12 [11].

Figure 24: Local coordinate system of a beam

$$
\mathbf{K} =
\begin{bmatrix}
\frac{EA}{L} \\
0 & \frac{12EI_z}{L^3(1+\Phi_y)} \\
0 & 0 & \frac{12EI_y}{L^3(1+\Phi_z)} & & & & Symmetric \\
0 & 0 & 0 & \frac{GJ}{L} \\
0 & 0 & -\frac{6EI_y}{L^2(1+\Phi_z)} & 0 & \frac{(4+\Phi_z)EI_y}{L(1+\Phi_z)} \\
0 & \frac{6EI_z}{L^2(1+\Phi_y)} & 0 & 0 & 0 & \frac{(4+\Phi_y)EI_z}{L(1+\Phi_y)} \\
-\frac{EA}{L} & 0 & 0 & 0 & 0 & 0 & \frac{EA}{L} \\
0 & -\frac{12EI_z}{L^3(1+\Phi_y)} & 0 & 0 & 0 & -\frac{6EI_z}{L^2(1+\Phi_y)} & 0 & \frac{12EI_z}{L^3(1+\Phi_y)} \\
0 & 0 & -\frac{12EI_y}{L^3(1+\Phi_z)} & 0 & \frac{6EI_y}{L^2(1+\Phi_z)} & 0 & 0 & 0 & \frac{12EI_y}{L^3(1+\Phi_z)} \\
0 & 0 & 0 & -\frac{GJ}{L} & 0 & 0 & 0 & 0 & 0 & \frac{GJ}{L} \\
0 & 0 & -\frac{6EI_y}{L^2(1+\Phi_z)} & 0 & \frac{(2-\Phi_z)EI_y}{L(1+\Phi_z)} & 0 & 0 & 0 & \frac{6EI_y}{L^2(1+\Phi_z)} & 0 & \frac{(4+\Phi_z)EI_y}{L(1+\Phi_z)} \\
0 & \frac{6EI_z}{L^2(1+\Phi_y)} & 0 & 0 & 0 & \frac{(2-\Phi_y)EI_z}{L(1+\Phi_y)} & 0 & -\frac{6EI_z}{L^2(1+\Phi_y)} & 0 & 0 & 0 & \frac{(4+\Phi_y)EI_z}{L(1+\Phi_y)}
\end{bmatrix}
\tag{12}
$$

$$\Phi_y = \frac{12EI_z}{GA_{s_y}l^2} = 24(1+\nu)\frac{A}{A_{s_y}}\left(\frac{r_z}{l}\right)^2 \tag{13}$$

$$\Phi_z = \frac{12EI_y}{GA_{s_z}l^2} = 24(1+\nu)\frac{A}{A_{s_z}}\left(\frac{r_y}{l}\right)^2 \tag{14}$$

In these equations A_s is the cross-sectional area which is effective in shear, and $\frac{r_z}{l}$ and $\frac{r_y}{l}$ are the ratios of the radius of gyration to the element length. If the latter are small compared to unity, as is the case with a slender beam, Φ_y and Φ_z can be considered zero [11]. In this case the effects of shear deformation are neglected and Euler-Bernoulli beam theory is applied. The Matlab model assumes slender beam elements.

Because the cross sections and lengths of the elements differ, several local stiffness and mass matrices are needed. The simplified local stiffness matrix of a beam element is shown in equation 15, the local mass matrix in equation 16 [11]. In the latter, m is the mass of the element and could be replaced with ρAL. Only half of the matrices are shown, since they are symmetric.

$$\mathbf{K} = \begin{bmatrix}
\frac{EA}{L} \\
0 & \frac{12EI_z}{L^3} \\
0 & 0 & \frac{12EI_y}{L^3} & & & & & \textit{Symmetric} \\
0 & 0 & 0 & \frac{GJ}{L} \\
0 & 0 & -\frac{6EI_y}{L^2} & 0 & \frac{4EI_y}{L} \\
0 & \frac{6EI_z}{L^2} & 0 & 0 & 0 & \frac{4EI_z}{L} \\
-\frac{EA}{L} & 0 & 0 & 0 & 0 & 0 & \frac{EA}{L} \\
0 & -\frac{12EI_z}{L^3} & 0 & 0 & 0 & -\frac{6EI_z}{L^2} & 0 & \frac{12EI_z}{L^3} \\
0 & 0 & -\frac{12EI_y}{L^3} & 0 & \frac{6EI_y}{L^2} & 0 & 0 & 0 & \frac{12EI_y}{L^3} \\
0 & 0 & 0 & -\frac{GJ}{L} & 0 & 0 & 0 & 0 & 0 & \frac{GJ}{L} \\
0 & 0 & -\frac{6EI_y}{L^2} & 0 & \frac{2EI_y}{L} & 0 & 0 & 0 & \frac{6EI_y}{L^2} & 0 & \frac{4EI_y}{L} \\
0 & \frac{6EI_z}{L^2} & 0 & 0 & 0 & \frac{2EI_z}{L} & 0 & -\frac{6EI_z}{L^2} & 0 & 0 & 0 & \frac{4EI_z}{L}
\end{bmatrix} \tag{15}$$

$$\mathbf{M} = m \begin{bmatrix}
\frac{1}{3} \\
0 & \frac{13}{35}+\frac{6I_z}{5AL^2} \\
0 & 0 & \frac{13}{35}+\frac{6EI_y}{5AL^2} & & & & & \textit{Symmetric} \\
0 & 0 & 0 & \frac{J}{3A} \\
0 & 0 & -\frac{11L}{210}-\frac{I_y}{10AL} & 0 & \frac{L^2}{105}+\frac{2I_y}{15A} \\
0 & \frac{11L}{210}+\frac{I_z}{10AL} & 0 & 0 & 0 & \frac{L^2}{105}+\frac{2I_z}{15A} \\
\frac{1}{6} & 0 & 0 & 0 & 0 & 0 & \frac{1}{3} \\
0 & \frac{9}{70}-\frac{6I_z}{5AL^2} & 0 & 0 & 0 & \frac{13L}{420}-\frac{I_z}{10AL} & 0 & \frac{13}{35}+\frac{6I_z}{5AL^2} \\
0 & 0 & \frac{9}{70}-\frac{6I_y}{5AL^2} & 0 & -\frac{13L}{420}+\frac{I_y}{10AL} & 0 & 0 & 0 & \frac{13}{35}+\frac{6I_y}{5AL^2} \\
0 & 0 & 0 & \frac{J}{6A} & 0 & 0 & 0 & 0 & 0 & \frac{J}{3A} \\
0 & 0 & \frac{13L}{420}-\frac{I_y}{10AL} & 0 & -\frac{L^2}{140}-\frac{I_y}{30A} & 0 & 0 & 0 & \frac{11L}{210}+\frac{I_y}{10AL} & 0 & \frac{L^2}{105}+\frac{2I_y}{15A} \\
0 & -\frac{13L}{420}+\frac{I_z}{10AL} & 0 & 0 & 0 & -\frac{L^2}{140}-\frac{I_z}{30A} & 0 & -\frac{11L}{210}-\frac{I_z}{10AL} & 0 & 0 & 0 & \frac{L^2}{105}+\frac{2I_z}{15A}
\end{bmatrix}$$
$$\tag{16}$$

C.2 Global stiffness and mass matrices

Local stiffness and mass matrices describe beam elements with the x-axis of the coordinate system in line with the length of the beam. To describe the elements in a global coordinate system, a rotation matrix $\mathbf{R}$ is needed. A beam element consists of two nodes with each six degrees of freedom, which means that the rotation matrix will have the size 12x12 (similar to the local stiffness and mass matrices). The following method to obtain the global stiffness and mass matrices has been developed in a previous assignment [12].

The 12x12 rotation matrix consists of all zeros, apart from four 3x3 rotation matrices on the diagonal. The 3x3 rotation matrices consist of three columns containing the unit base vectors. The first unit base vector $\mathbf{e}_x$ is calculated by subtracting the coordinates of the first node from the coordinates of the second node and dividing this by the length of the beam element.

The local y-axis is determined to be always horizontal. This means that the second unit base vector $\mathbf{e}_y$ can be calculated using the cross product between $\mathbf{e}_x$ and the global z-axis $\mathbf{e}_{z0}$ and dividing by its length, where $\mathbf{e}_{z0} = \begin{bmatrix} 0 & 0 & 1 \end{bmatrix}^T$.

The third unit base vector can be calculated with the cross product of the first two: $\mathbf{e}_z = \mathbf{e}_x \times \mathbf{e}_y$.
For the elements which are rotated 90 degrees, the 3x3 rotation matrices are added manually.

The stiffness matrices are rotated to the global coordinate system using equation 17. The mass matrices are rotated in a similar way.

$$\mathbf{K}_{uncoupled} = \mathbf{R}\mathbf{K}\mathbf{R}^T \tag{17}$$

A Boolean matrix $\mathbf{B}$ has been used to connect the elements. The Boolean matrix is of size 120x66. The total number of degrees of freedom is 1020 (85 elements with each 12 dof) and 300 is the number of independent degrees of freedom (50 nodes with each 6 dof). The Boolean matrix consists mainly of zeros, with ones at the intersections of the elements. The coupled stiffness matrix is calculated using equation 18. Again, the coupled mass matrix is calculated in a similar way.

$$\mathbf{K}_{coupled} = \mathbf{B}^T \mathbf{K}_{uncoupled} \mathbf{B} \tag{18}$$

C.3 Stiffness and mass matrices from Ansys

Stiffness and mass matrices can also be obtained directly from an Ansys model. The location of the nodes is defined as well as the connecting elements, where each different cross section needs a different element type. Constraints are set such that all deformations of the bottom four nodes are set to zero.

After solving this analysis, the stiffness and mass matrices can be extracted. However, Ansys changes the order of nodes such that the model can be evaluated as efficiently as possible, which is called solver ordering [13]. To be able to compare these matrices to the ones written in Matlab, they should be reconverted to user ordering. For this purpose conversion vectors are extracted from Ansys.

C.4 Evaluation

This model can be evaluated using the equation of motion 19. In this equation $\ddot{\mathbf{u}}$ is the acceleration, $\dot{\mathbf{u}}$ is the velocity and $\mathbf{u}$ the displacement of the nodes, while $\mathbf{P}$ is the load vector, containing all forces and moments acting on the nodes. The damping matrix $\mathbf{C}$ can be added as the stiffnessmatrix multiplied with a (small) constant. Naturally, the first two terms of this equation are left out in static analysis.

$$\mathbf{M}\ddot{\mathbf{u}} + \mathbf{C}\dot{\mathbf{u}} + \mathbf{K}\mathbf{u} = \mathbf{P} \tag{19}$$

This equation is first inversed to calculate the displacement of the nodes. In dynamic evaluation the Newmark-β integration scheme is used for this purpose, as elaborated in appendix F. The boundary condition in this model is that the bottom four nodes have a rigid connection to the ground (nodes 1, 2, 19 and 20). Therefore these entries are removed from the stiffness and mass matrices.

Once the displacement is known, the total matrices are again used to determine the reaction forces.

D Limitations of the Ansys-Adams interface

MSC Adams is a software package which can be used to simulate the dynamics of a multibody system. As default it assumes all components to be rigid, and tools to model flexibility only exist for simple structures. If the flexible component has a more complex geometry, Adams requires data obtained from finite element programs [13].

In this thesis the Ansys-Adams interface is used to obtain a flexible multibody model. A model of the structure is built in Solidworks, which is then imported into Adams, to model the motion of the multibody system. Ansys is used to obtain the data necessary to make a part flexible. There are two ways to obtain this data.

The first option is to import the SolidWorks part into Ansys and mesh it (usually with solid elements). Interface nodes are added at the location of constraints, applied forces and the end of the structure. Often a rigid region is added to these interface nodes, to distribute applied loads. The ADAMS command is used to write flexible body information to a modal neutral file (.mnf), which can be imported into Adams [13].

The second option is to manually model the structure in Ansys. This enables the use of beam elements, which can greatly simplify the model and thus decrease computational effort. In this method no rigid regions are necessary.

D.1 Simple beam

To test the validity of this method, a simple beam model is used. The beam has a length of 10 m and a solid circular cross section with a radius of 0,05 m. One end of the beam is clamped, while the load is applied at the other end. The beam is divided into 10 beam elements (apart from the one modelled with solid elements).

The applied load consists of a force in negative z-direction of 100 kN and a moment around the y-axis of 100 kNm, as shown in figure 25. The deformed beam according to the different models is shown in figure 26 and the location of the end of the beam is noted in table 3. Note that the z-axis in Matlab is vertical, where in Ansys and Adams it is horizontal (in these models the vertical axis is the y-axis). It is clear that the models of Matlab and Ansys give the same result, while the results in Adams are very different. The Adams models using solid and beam elements give the same results, which is why only one of these figures is shown.
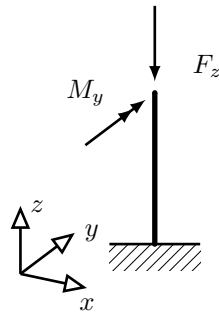

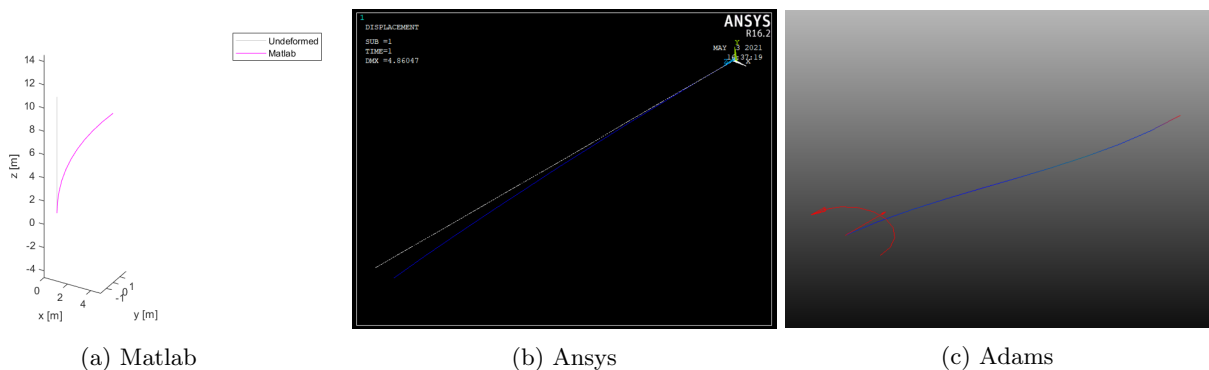Figure 25: Load case of the simple beam

(a) Matlab (b) Ansys (c) Adams

Figure 26: Deformation of a single beam

Table 3: Location of the end of the beam after deformation [m]

	x	y	z
Matlab	4,85	0	10
Ansys	4,86	0	10
Adams solid	-2,31	0	9,74
Adams beam	-2,31	0	9,74

D.2 Other load cases

Several different load cases are used to determine the range of applied loads for which the models are valid. Firstly, a load containing only forces is applied. The force in x-direction is 10 kN, the force in y-direction is 20 kN and the force in z-direction is 30 kN. The results are shown in the top row of table 4. It can be seen that the Adams model gives again different results.

However, the application of smaller loads clearly shows the linearity of the Matlab and Ansys models, which makes them only valid for small deformations. Table 4 shows that for smaller loads (both forces and moments) all models provide the same results.

Table 4: Location of the end of the beam after deformation with loads of varying magnitude [m]

Load F [N] and M [Nm]						Matlab			Ansys			Adams		
F_x	F_y	F_z	M_x	M_y	M_z	x	y	z	x	y	z	x	y	z
10000	20000	30000	0	0	0	3,23	6,47	0	3,24	6,48	0	1,46	2,91	-0,54
1000	2000	3000	0	0	0	0,32	0,65	0	0,32	0,65	0	0,29	0,59	-0,02
100	200	300	0	0	0	0,032	0,065	0	0,032	0,065	0	0,032	0,064	0
200	0	0	0	-100	0	0,060	0	0	0,060	0	0	0,060	0	0

D.3   Simple structure

A simple structure as seen in figure 27 is used to compare results in Matlab and Adams. A load of $F_x = 1f$ N, $F_y = 2f$ N and $F_z = 3f$ N is applied at the highlighted node and the three bottom nodes are fixed, either directly or using a rigid region in the mnf file. The deformation of the same node for different load cases and boundary conditions are listed in table 5.
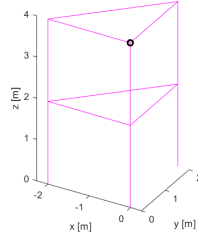

Figure 27: Simple structure

Table 5: Deformation of the highlighted node of the simple structure [mm]

	f	x	y	z
Matlab	100	68,2	143,7	0
Adams	100	66,5	138,3	-2,1
Adams rigid region	100	66,6	137,5	-2,1
Matlab	10	6,8	14,4	0
Adams	10	6,8	14,3	0
Adams rigid region	10	6,8	14,3	0

D.4 Wirbelbaum

The static load case of the Wirbelbaum as shown in figure 28 is repeated for several orders of magnitude. The deformation of the four top nodes is shown in tables 6 and 7. The deformations appears to be linearly dependent on the applied load, though the Adams model loses some accuracy for smaller deformations.

It can be seen that a difference between the Matlab and Adams models remains, even though the deformations can be considered small.
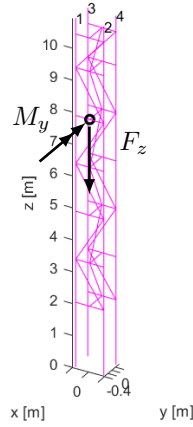

Figure 28: Visualisation of the static load case

Table 6: Deformation of the four top nodes [mm] for $F_y = -100000$ N and $M_z = 100000$ Nm

Node	Matlab			Adams		
	x	y	z	x	y	z
1	8,3	-4,8	0,3	6,1	-3,8	0,1
2	8,3	-1,1	-0,9	6,1	-1,6	-0,7
3	1,9	-4,9	0,1	4,3	-3,8	0,3
4	1,9	-1,0	-0,1	4,3	-1,6	-0,3

Table 7: Deformation of the four top nodes [mm] for $F_y = -10000$ N and $M_z = 10000$ Nm

Node	Matlab			Adams		
	x	y	z	x	y	z
1	0,83	-0,48	0,03	0,60	-0,40	0
2	0,83	-0,11	-0,09	0,60	-0,20	-0,10
3	0,19	-0,49	0,01	0,40	-0,40	0
4	0,19	-0,10	-0,01	0,40	-0,20	0

E Equivalent Load

The load exerted by the gondolas on the tower of the Wirbelbaum moves up and down. When this load is located in between two nodes, it should be transformed into equivalent loads on these two nearest nodes. This transformation can be done by multiplication with interpolation functions, which uses the dimensionless length $\xi = \frac{x}{L}$.

This appendix explains how this transformation can be performed. For this purpose a 2D beam element is used.

E.1 Force in x-direction

The transformation of the force in x-direction is the easiest. If for example the force is located at the left node, the multiplication in the left node should be 1, while it is 0 at the right node (and vice versa). This can be described by a linear function, which results in equation 20.

$$\mathbf{P}_{eq} = \begin{bmatrix} F_{x1} \\ F_{x2} \end{bmatrix} = \begin{bmatrix} 1 - \xi \\ \xi \end{bmatrix} F_x \tag{20}$$

E.2 Force in y-direction

The interpolation functions necessary to transform a force in y-direction are determined using an example of a beam. The deflection and rotation of the beam with a force in y-direction at location x (figure 29) should equal those of the beam with a force and moment at the end (figure 30). Thus, the corresponding equations for the deflection (equations 21 and 23) should be equal to each other. The same holds for the equations for the rotation (equations 22 and 24).

Note that the deformation of the beam in figure 30 is not realistic. This method states that only the deformations at the nodes should be equal, the shape in between is irrelevant.
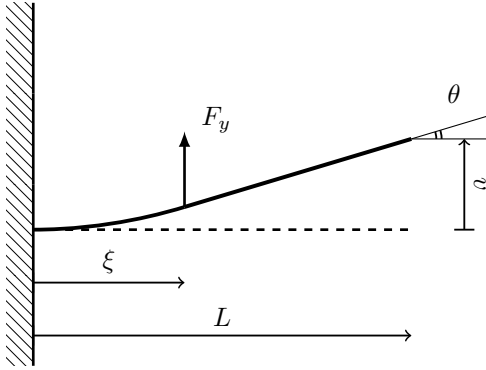

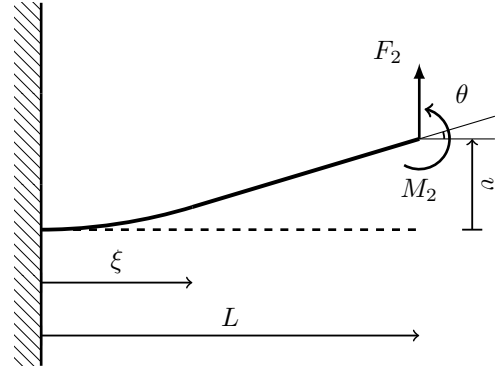Figure 29: Actual loading situation F_y

Figure 30: Equivalent load caused by F_y

$$v = \frac{Fx^3}{3EI} + (L - x)\frac{Fx^2}{2EI} \tag{21}$$

$$\theta = \frac{Fx^2}{2EI} \tag{22}$$

$$v = \frac{F_2 L^3}{3EI} + \frac{M_2 L^2}{2EI} \tag{23}$$

$$\theta = \frac{F_2 L^2}{2EI} + \frac{M_2 L}{EI} \tag{24}$$

Rewriting these equations and replacing $\frac{x}{L}$ with ξ describes the equivalent force in the right node as a function of F_y and ξ. The reaction force and moment in the left node can be determined using equilibrium equations. Written in matrix form, this results in equation 25.

$$\mathbf{P}_{eq} = \begin{bmatrix} F_{y1} \\ M_{z1} \\ F_{y2} \\ M_{z2} \end{bmatrix} = \begin{bmatrix} 1 - 3\xi^2 + 2\xi^3 \\ L(\xi - 2\xi^2 + \xi^3) \\ 3\xi^2 - 2\xi^3 \\ L(-\xi^2 + \xi^3) \end{bmatrix} F_y \tag{25}$$

It can be verified that for $\xi = 0$ only F_{y1} is nonzero and equal to F. For $\xi = 1$ only F_{y2} is nonzero and equal to F.

E.3 Moment

The interpolation functions necessary to transform a moment around the z-axis are determined in a similar way. The visualisation of the example is shown in figure 31 and 32. The corresponding equations for the deflection are shown in equations 26 and 28 and those for the rotation in equations 27 and 29. Again, the surrealistic deformation along the beam in figure 32 is irrelevant for this calculation.
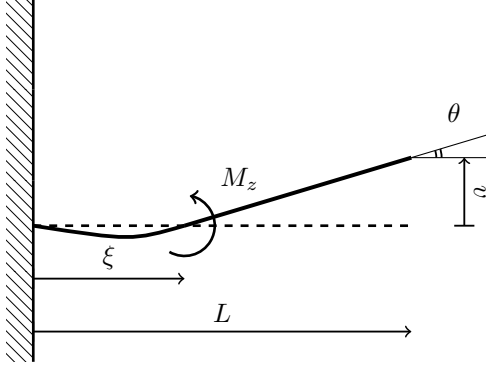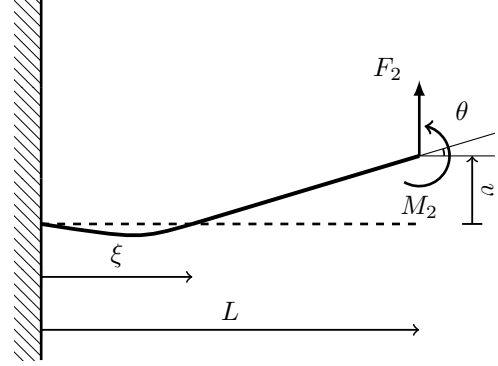

Figure 31: Actual loading situation M_z

Figure 32: Equivalent load caused by M_z

$$v = \frac{Mx^2}{2EI} + (L - x)\frac{Mx}{EI} \qquad (26)$$

$$\theta = \frac{Mx}{EI} \qquad (27)$$

$$v = \frac{F_2 L^3}{3EI} + \frac{M_2 L^2}{2EI} \qquad (28)$$

$$\theta = \frac{F_2 L^2}{2EI} + \frac{M_2 L}{EI} \qquad (29)$$

These equations can be rewritten in a similar fashion to obtain the equivalent force in the right node as a function of the original moment M_z and ξ. Again, the reaction force and moment in the left node can be obtained using equilibrium equations. The result is shown in equation 30.

$$\mathbf{P}_{eq} = \begin{bmatrix} F_{y1} \\ M_{z1} \\ F_{y2} \\ M_{z2} \end{bmatrix} = \begin{bmatrix} -\frac{1}{L}(6\xi - 6\xi^2) \\ 1 - 4\xi + 3\xi^2 \\ \frac{1}{L}(6\xi - 6\xi^2) \\ -2\xi + 3\xi^2 \end{bmatrix} M_z \qquad (30)$$

This equation can be verified as well. For $\xi = 0$, only M_{z1} is nonzero and equal to M_z. The same holds for M_{z2} when $\xi = 1$.

E.4 Equivalent load in 3D

Determining the equivalent load in a 3D situation is mostly very similar. The matrix entries for the force in z-direction equal those for the force in y-direction and the same goes for the moments in y- and z-direction. The only thing that must be added is an expression for the torsional moment M_x, but its requirements are equal to those of the force in x-direction. Therefore this relation can be described by the same linear function shown in equation 31.

$$\mathbf{P}_{eq} = \begin{bmatrix} M_{x1} \\ M_{x2} \end{bmatrix} = \begin{bmatrix} 1 - \xi \\ \xi \end{bmatrix} M_x \qquad (31)$$

All the shape functions are collected in a single matrix $\mathbf{A}$, which can be multiplied with the original load vector to obtain the equivalent load vector. This final result is shown in equation 32.

$$
\mathbf{P}_{eq} = \mathbf{AP} = \begin{bmatrix}
1-\xi & 0 & 0 & 0 & 0 & 0 \\
0 & 1-3\xi^2+2\xi^3 & 0 & 0 & 0 & -\frac{1}{L}(6\xi-6\xi^2) \\
0 & 0 & 1-3\xi^2+2\xi^3 & 0 & -\frac{1}{L}(6\xi-6\xi^2) & 0 \\
0 & 0 & 0 & 1-\xi & 0 & 0 \\
0 & 0 & L(\xi-2\xi^2+\xi^3) & 0 & 1-4\xi+3\xi^2 & 0 \\
0 & L(\xi-2\xi^2+\xi^3) & 0 & 0 & 0 & 1-4\xi+3\xi^2 \\
\xi & 0 & 0 & 0 & 0 & 0 \\
0 & 3\xi^2-2\xi^3 & 0 & 0 & 0 & \frac{1}{L}(6\xi-6\xi^2) \\
0 & 0 & 3\xi^2-2\xi^3 & 0 & \frac{1}{L}(6\xi-6\xi^2) & 0 \\
0 & 0 & 0 & \xi & 0 & 0 \\
0 & 0 & L(-\xi^2+\xi^3) & 0 & -2\xi+3\xi^2 & 0 \\
0 & L(-\xi^2+\xi^3) & 0 & 0 & 0 & -2\xi+3\xi^2
\end{bmatrix}
\begin{bmatrix}
F_x \\
F_y \\
F_z \\
M_x \\
M_y \\
M_z
\end{bmatrix} \quad (32)
$$

F Newmark-β integration

The Newmark-β integration scheme is used to compute the displacements, velocities and accelerations of all the nodes at the next time step [14]. This integration scheme is implicit (except when $\beta = 0$), which means that the current displacement is related to the current acceleration, as well as the response from the previous time step. The main advantage of implicit integration schemes is their unconditional stability, though explicit methods are more computationally efficient. Numerical damping can be added to suppress instabilities of the higher mode responses [15].

The equilibrium equation 33 includes the mass matrix $\mathbf{M}$, acceleration $\ddot{\mathbf{u}}$, damping matrix $\mathbf{C}$, velocity $\dot{\mathbf{u}}$, stiffness matrix $\mathbf{K}$, displacement $\mathbf{u}$ and load $\mathbf{P}$ of the structure. The damping matrix is proportional to the stiffness matrix.

$$\mathbf{M}\ddot{\mathbf{u}} + \mathbf{C}\dot{\mathbf{u}} + \mathbf{K}\mathbf{u} = \mathbf{P} \tag{33}$$

Newmarks equations for the velocity $\dot{\mathbf{u}}$ and displacement $\mathbf{u}$ at time $t = t + \Delta t$ are given in equations 34 and 35 respectively, with β as the Newmark-β parameter $(\beta = \frac{1}{4})$ and γ as the Newmark numerical damping parameter $(\gamma = \frac{1}{2})$.

$$\dot{\mathbf{u}}_{t+\Delta t} = \dot{\mathbf{u}}_t + \Delta t\left((1-\gamma)\ddot{\mathbf{u}}_t + \gamma\ddot{\mathbf{u}}_{t+\Delta t}\right) \tag{34}$$

$$\mathbf{u}_{t+\Delta t} = \mathbf{u}_t + \Delta t\dot{\mathbf{u}}_t + \Delta t^2\left(\left(\frac{1}{2} - \beta\right)\ddot{\mathbf{u}}_t + \beta\ddot{\mathbf{u}}_{t+\Delta t}\right) \tag{35}$$

It can be seen that both the velocity and the displacement depend on values from the previous time step and the acceleration $\ddot{\mathbf{u}}$ of the current time step. Equation 35 can be rewritten to obtain an equation for the acceleration, as shown in equation 36.

$$\ddot{\mathbf{u}}_{t+\Delta t} = \frac{1}{\beta\Delta t^2}\mathbf{u}_{t+\Delta t} - \frac{1}{\beta\Delta t^2}\mathbf{u}_t - \frac{1}{\beta\Delta t}\dot{\mathbf{u}}_t - \left(\frac{1}{2\beta} - 1\right)\ddot{\mathbf{u}}_t \tag{36}$$

This equation depends on values form the previous time step and the current displacement. When the result is put into equation 34, the result is an equation for the new velocity in terms of previous results and the current displacement (equation 37).

$$\dot{\mathbf{u}}_{t+\Delta t} = \frac{\gamma}{\beta\Delta t}\mathbf{u}_{t+\Delta t} - \frac{\gamma}{\beta\Delta t}\mathbf{u}_t + \left(1 - \frac{\gamma}{\beta}\right)\dot{\mathbf{u}}_t + \Delta t\left(1 - \frac{\gamma}{2\beta}\right)\ddot{\mathbf{u}}_t \tag{37}$$

The current displacement can also be obtained by rewriting equation 33, as shown in equation 38.

$$\mathbf{u}_{t+\Delta t} = \mathbf{K}^{-1}\left(\mathbf{P}_{t+\Delta t} - \mathbf{M}\ddot{\mathbf{u}}_{t+\Delta t} - \mathbf{C}\dot{\mathbf{u}}_{t+\Delta t}\right) \tag{38}$$

Equation 37 is used to replace $\dot{\mathbf{u}}$ in equation 38, equation 36 is used to replace $\ddot{\mathbf{u}}$, and the obtained equation is rewritten, which results in a new equation for the current displacement. This equation is shown in equation 39.

$$\mathbf{u}_{t+\Delta t} = \left(\mathbf{K} + \mathbf{M}\frac{1}{\beta\Delta t^2} + \frac{\mathbf{C}\gamma}{\beta\Delta t}\right)^{-1}\left(\mathbf{P}_{t+\Delta t} + \mathbf{M}\left(\frac{1}{\beta\Delta t^2}\mathbf{u}_t + \frac{1}{\beta\Delta t}\dot{\mathbf{u}}_t + \left(\frac{1}{2\beta} - 1\right)\ddot{\mathbf{u}}_t\right) + \mathbf{C}\left(\frac{\gamma}{\beta\Delta t}\mathbf{u}_t - \left(1 - \frac{\gamma}{\beta}\right)\dot{\mathbf{u}}_t - \Delta t\left(1 - \frac{\gamma}{2\beta}\right)\ddot{\mathbf{u}}_t\right)\right) \tag{39}$$

Since equation 39 depends only on values from the previous time step and the known force vector, this can be calculated firstly (the displacement, velocity and acceleration at $t = 0$ are zero). Secondly the acceleration is calculated using equation 36 and thirdly the velocity is calculated using equation 37. This is repeated for every time step.